The Astrophysical Journal, 956:29 (16pp), 2023 October 10 https://doi.org/10.3847/1538-4357/ace9b6

Prospects for Cryovolcanic Activity on Cold Ocean Planets

Lynnae C. Quick[1,2,3], Aki Roberge[1,2,3], Guadalupe Tovar Mendoza[2,4,5,6], Elisa V. Quintana[1,2], and Allison A. Youngblood[1]
[1] NASA Goddard Space Flight Center, 8800 Greenbelt Road, Greenbelt, MD 20771, USA; Lynnae.C.Quick@nasa.gov
[2] The Nexus for Exoplanet System Science (NExSS), USA
[3] The Network for Ocean Worlds (NOW), USA
[4] Department of Astronomy, University of Washington, Seattle, WA, 98195, USA
[5] Astrobiology Program, University of Washington, Box 351580, Seattle, WA 98195, USA
Received 2023 April 28; accepted 2023 July 16; published 2023 October 4

Abstract

We have estimated total internal heating rates and depths to possible subsurface oceans for 17 planets that may be cold ocean planets, low-mass exoplanets with equilibrium surface temperatures and/or densities that are consistent with icy surfaces and a substantial H_2O content. We have also investigated the potential for tidally driven cryovolcanism and exosphere formation on these worlds. Estimated internal heating rates from tidal and radiogenic sources are large enough that all planets in our study may harbor subsurface oceans, and their geological activity rates are likely to exceed the geological activity rates on Jupiter's moon Europa. Several planets are likely to experience enhanced volcanic activity rates that exceed that of Io. Owing to their relatively thin ice shells and high rates of internal heating, Proxima Cen b and LHS 1140 b are the most favorable candidates for telescopic detection of explosive, tidally driven cryovolcanism. Estimates for thin ice shells on Proxima Cen b, LHS 1140 b, Trappist-1f, and several Kepler planets suggest that any H_2O vented into space during explosive cryovolcanic eruptions on these worlds could be sourced directly from their subsurface oceans. Like the icy moons in our outer solar system, cold ocean planets may be astrobiologically significant worlds that harbor habitable environments beneath their icy surfaces. These possibilities should be considered during analyses of observational data for small exoplanets from current and upcoming telescopes and during planning for a future space telescope mission aimed at characterization of potentially habitable exoplanets (e.g., Habitable Worlds Observatory).

Unified Astronomy Thesaurus concepts: Exoplanet tides (497); Exoplanet surfaces (2118); Volcanism (2174); Exoplanet surface characteristics (496); Exoplanet atmospheres (487); Habitable planets (695); Exoplanets (498); Super Earths (1655); Ocean planets (1151)

1. Introduction

Ocean planets are a proposed class of low-density, terrestrial exoplanets with substantial liquid water layers (Léger et al. 2004). They may exist in a variety of climactic states including ice free, partially ice covered, or completely frozen over at their surfaces (Budyko 1969; Sellers 1969; Tajika 2008). Here, as in Quick et al. (2020), we refer to ocean-bearing planets with ice-covered surfaces as *cold ocean planets*. Cold ocean planets may be plentiful in extrasolar planetary systems and common throughout the Galaxy (Ehrenreich et al. 2006; Ehrenreich & Cassan 2007; Quick et al. 2020; Tjoa et al. 2020); their interior structures and compositions may resemble those of the large icy moons in our outer solar system (Tajika 2008; Fu et al. 2010; Vance et al. 2015; Yang et al. 2017; Ribas et al. 2018; Vance et al. 2020; Kane et al. 2021). Despite their ice-covered surfaces, these planets may be astrobiologically significant worlds, with habitable environments in subsurface oceans (Heller & Armstrong 2014; Wilhelm et al. 2022) or in water-filled reservoirs perched within their ice shells (e.g., see Fagents et al. 2000; Schmidt et al. 2011; Muñoz-Iglesias et al. 2013; Manga & Michaut 2017; Lesage et al. 2020; Chivers et al. 2021; Quick et al. 2021). Indeed, both of these scenarios are possible for Jupiter's moon Europa (Ruiz et al. 2007; Hand et al. 2009).

Ocean planets situated within the conventional stellar habitable zone may become cold ocean planets with fully or partially ice-covered surfaces if volcanism is sporadic, if CO_2 supply rates from volcanism or preexisting atmospheric CO_2 levels are low (Tajika 2008; Ding & Wordsworth 2020; Krissansen-Totton et al. 2021), or if surface oceans serve as CO_2 sinks (Tajika 2008). Indeed, Earth may have existed in ice-covered "snowball" states for a total of up to 10% of its history (Tajika 2008). Our home planet experienced at least three of these cold ocean planet cycles, including one in which life may have persisted under a 1 km thick ice shell (Wilhelm et al. 2022). Recent studies have suggested that even mostly ice-covered planets can have substantial amounts of unfrozen land near their equators or small, equatorial regions of salt-rich water (Del Genio et al. 2019; Paradise et al. 2019) where life could flourish. Hence, akin to the ocean worlds in our solar system, cold ocean planets represent potentially habitable worlds of astrobiological significance in extrasolar planetary systems.

If the internal structures of cold ocean planets indeed resemble those of the ice-covered ocean moons in our outer solar system (see Vance et al. 2007, 2015; Journaux et al. 2017, 2020; Kane et al. 2021), then geophysical processes operating on these worlds may be similar to geophysical processes operating on our solar system's icy moons and may

[6] NSF Graduate Fellow.

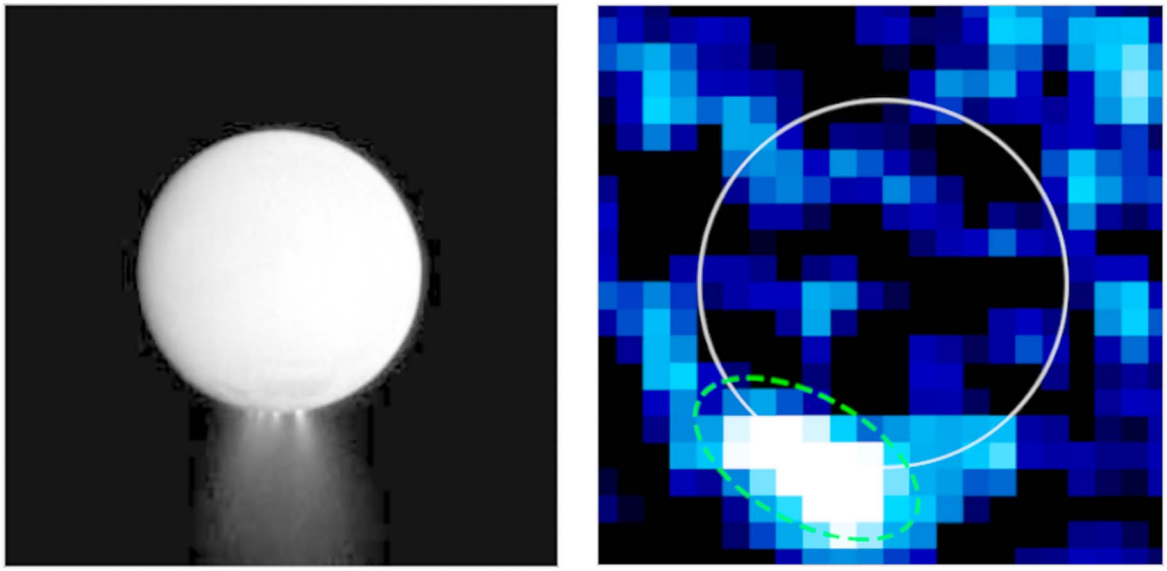

Figure 1. Explosive cryovolcanism in the form of geyser-like plumes on two of our solar system's ocean worlds. Left: Cryovolcanic eruptions at the south pole of Saturn's moon Enceladus (credit: NASA/JPL-Caltech/SSI). Right: Hubble Space Telescope UV observations of cryovolcanic eruptions at the south pole of Jupiter's moon Europa (credit: NASA/L. Roth). By facilitating the transport of liquid water and energy between their interiors and surfaces, similar activity could create habitable environments on cold ocean planets.

include ice tectonics and cryovolcanism (Fu et al. 2010; Levi et al. 2013, 2014; Quick et al. 2017; Barr et al. 2018; Quick et al. 2020). Cryovolcanism is the eruption of liquid or vapor phases of water, or other aqueous solutions, that would be frozen at the normal temperature of an icy satellite or planet's surface (Geissler 2000). Effusive cryolava flows and/or evidence for cryovolcanic eruption products exist on numerous H_2O-rich bodies in our solar system including Ceres (Ruesch et al. 2016, 2019; Quick et al. 2019), Europa (Fagents et al. 2000; Fagents 2003; Quick et al. 2017, 2022), Titan (Lopes et al. 2013), Triton (Smith et al. 1989; Soderblom et al. 1990), Ariel (Jankowski & Squyres 1988; Croft & Soderblom 1991; Schenk 1991; Cartwright et al. 2020; Beddingfield & Cartwright 2021), Miranda (Jankowski & Squyres 1988; Schenk 1991), Pluto (Moore et al. 2016; Cruikshank et al. 2019, 2021; Martin & Binzel 2021; McGovern et al. 2021; Singer et al. 2022), and Charon (Beyer et al. 2019).

Explosive cryovolcanism, in the form of internally sourced geyser-like plumes, has been detected on Enceladus (Porco et al. 2006; Spencer et al. 2006) and Europa (Roth et al. 2014a; Sparks et al. 2016, 2017) (Figure 1). Neptune's moon Triton may also host internally sourced explosive cryovolcanism (Hansen et al. 2021; Hofgartner et al. 2022). All of these moons harbor internal oceans beneath layers of surface ice (Carr et al. 1998; Kivelson et al. 2000; Ruiz 2003; Nimmo & Pappalardo 2016; Thomas et al. 2016; Hansen et al. 2021). The maintenance of subsurface oceans and geological activity on these worlds is a direct consequence of the tidal energy they receive from their host planets (e.g., Ojakangas & Stevenson 1989; Sotin et al. 2002; Hurford et al. 2007; Roberts & Nimmo 2008; Gaeman et al. 2012; Chen et al. 2014; Rhoden et al. 2015), and energy resulting from tidal and radiogenic heating facilitates the continuous cycling of liquid water and organics (see Postberg et al. 2009, 2011, 2018) between their surfaces and interiors via cryovolcanism (Fagents et al. 2000; Běhounková et al. 2015; Quick & Marsh 2016; Thomas et al. 2016; Hammond et al. 2018). Similarly, internal heating due to tidal and radiogenic effects may also facilitate the preservation of liquid layers and the maintenance of habitable conditions on cold ocean planets (Heller & Armstrong 2014).

Owing to their ice-covered surfaces and high albedos, cold ocean planets will be brighter in reflected light than comparably sized planets with bare rock or liquid water surfaces at similar orbital separations from their host stars (Kaltenegger et al. 2013; Wolf 2017). A substantial population of potential cold ocean planets might therefore be found in direct imaging surveys undertaken with powerful, next-generation telescopes. Given the constraints of remote sensing from interstellar distances, cryovolcanic signatures—such as temporally varying excesses of H_2O, O_2, O, and/or H (Bourrier et al. 2017; Quick et al. 2017)—may be the only way to determine whether an exoplanet is in fact a cold ocean planet with enough energy and liquid water to support a subsurface habitable environment.

2. Models

Given the expected similarities in composition, internal structure, and geophysical activity between the icy ocean worlds in our solar system and cold ocean planets in exoplanetary systems (Fu et al. 2010; Henning et al. 2018; Hurford et al. 2020; Quick et al. 2020), models employed to constrain the depth to subsurface oceans and determine rates of cryovolcanic activity on our solar system's icy moons may be used to place constraints on the availability and accessibility of liquid water and energy in the interiors of cold ocean planets. In the context of this study, we define cold ocean planets as exoplanets with masses (M_p) $\leqslant 8M_\oplus$ and radii (R_p) that are less than or approximately equal to $2R_\oplus$; this increases the likelihood that the planets we consider are solid rather than gas-rich sub-Neptunes (e.g., Stevenson 1982; Seager et al. 2007; Fabrycky et al. 2014; Rogers 2015).

In the absence of an atmosphere, Earth's equilibrium temperature is 255 K (Sagan & Mullen 1972). We therefore assume that equilibrium temperatures <255 K represent a plausible range of equilibrium surface temperatures for cold ocean planets, consistent with conditions that would allow for

Table 1
Cold Ocean Planets

Planet	$M_p(M_\oplus)$	$R_p(R_\oplus)$	ρ (kg m^{-3})	g (m s^{-2})	a (au)	e	P (days)	T_S (K)
GJ 514 b	5.2	2	3529	12.6	0.422	0.45	140.43	202
HD33793 c (Kapteyn c)	7	2.25	3375.8	13.5	0.311	0.23	121.54	See Table 3
Kepler 62 f[a]	1.5	1.461	2642.2	6.88	0.718	unknown	267.3	208
Kepler 296 f[a]	3	1.8	2809	9.03	0.255	0.33	63.3	See Table 3
Kepler 441 b[a]	2	1.64	2454	7.2	0.64	0.1	207.25	See Table 3
Kepler 442 b[a]	0.9	1.34	2054.8	4.91	0.409	0.04	112.3	See Table 3
Kepler 1229 b[a]	1.5	1.37	3202.2	7.8	0.3006	unknown	86.83	212
Kepler 1544 b[a]	3	1.79	2884.4	9.17	0.5421	unknown	168.82	269
Kepler 1652 b[a]	2	1.6	2677.1	7.65	0.1654	unknown	38.1	268
MOA-2007-BLG-192L b	3.2	1.7	3577.96	10.8	0.62	unknown	615.17	See Table 3
LHS 1140 b[a]	6.4	1.6	7857	23	0.0957	0.096	24.74	235
OGLE-2005-BLG-390-Lb	5.5	1.8	5180.6	16.62	2.6	unknown	3285	50
OGLE-2013-BLG-0341LB b	2	1.5	3255.3	8.7	0.702	unknown	679.31	See Table 3
Proxima Cen b	1.173	1.3	2932.92	6.79	0.04864	0.109	11.18	234
Trappist-1f[a]	1.039	1.045	4900	9.32	0.02925	0.0051	9.2	219
Trappist-1g[a]	1.321	1.129	5060	10.2	0.04683	0.00208	12.35	198.6
Trappist-1h[a]	0.326	0.755	4160	5.6	0.06189	0.00567	18.8	168

Note. Data extracted from the NASA Exoplanet Archive and references therein, namely, Beaulieu et al. (2006), Gould et al. (2014), Seager et al. (2007), Bennett et al. (2008), Kubas et al. (2012), Borucki et al. (2013, 2018), Anglada-Escudé et al. (2014, 2016), Barclay et al. (2015), Torres et al. (2015, 2017), Gillon et al. (2017), Grimm et al. (2018), Ment et al. (2019), Lillo-Box et al. (2020), Mascareño et al. (2020), Agol et al. (2021), Damasso et al. (2022).
[a] Denotes transiting planets.

Table 2
Stellar Properties

Star	L_* ($L_{\rm Sun}$)	$R_*(R_{\rm Sun})$	T_* (K)	Spectral Type	Average System Age (Gyr)
GJ 514	0.0398	0.5	3728	M	0.8
HD33793 (Kapteyn)	1×10^{-2}	0.29	3550	M	12
Kepler 62	0.264	0.73	4842	K	7
Kepler 296	2.7×10^{-2}	0.426	3572	M	4.2
Kepler 441	8.05×10^{-2}	0.55	4340	K	1.9
Kepler 442	0.117	0.598	4402	K	2.9
Kepler 1229	5.9×10^{-2}	0.57	3774	M	1.5
Kepler 1544	0.229	0.657	4937	K	3.9
Kepler 1652	2.3×10^{-2}	0.382	3638	M	3.2
LHS 1140	3.24×10^{-3}	0.21	2988	M	5
MOA-2007-BLG-192L	5.25×10^{-4}	0.113	2570	M	10.42
OGLE-2005-BLG-390-L	7.2×10^{-3}	0.268	3210	K	9.587
OGLE-2013-BLG-0341LB	3.02×10^{-3}	0.191	3060	M	10
Proxima Cen	1.55×10^{-3}	0.141	3050	M	4.8
Trappist-1	5.5×10^{-4}	0.1192	2566	M	8

Note. Data extracted from the NASA Exoplanet Archive and references therein, namely, Baraffe & Chabrier (1996), Gizis (1997), Baraffe et al. (2003), Beaulieu et al. (2006), Bennett et al. (2008), Haywood (2008), Kubas et al. (2008, 2012), Pierrehumbert & Gaidos (2011), Borucki et al. (2013, 2018) , Anglada-Escudé et al. (2014, 2016), Gould et al. (2014), Torres et al. (2015, 2017), Bazot et al. (2016), Ribas et al. (2016), Safonova et al. (2016), Luger et al. (2017), Stassun et al. (2019), Lillo-Box et al. (2020), Agol et al. (2021), Damasso et al. (2022), Mamajek (2022).

the long-term maintenance of ice-covered surfaces. In Quick et al. (2020), densities of cold ocean planets were assumed to range from 1000 to 3500 kg m^{-3}, corresponding to the density range of our solar system's icy moons (Jacobson et al. 1992; Anderson et al. 1997; Hussmann et al. 2006). However, solid planets with densities >3500 kg m^{-3} could have icy surfaces if their equilibrium temperatures are less than 255 K. If these worlds are subjected to tidal heating from their parent stars and/or have relatively high radiogenic heating rates, they may also harbor internal oceans. Thus, the upper end of the density range for cold ocean planets is increased in this study.

The physical properties of the exoplanets we have considered, including literature values for their average equilibrium temperatures, T_S, are displayed in Table 1; the properties of their host stars are displayed in Table 2. Planetary and host star data were extracted from the NASA Exoplanet Archive and references therein (see Tables 1 and 2 captions). Host star data were also extracted from Pecaut & Mamajek (2013) and Mamajek (2022).[7] Mean semimajor axis (a) and eccentricity (e) values have been employed for all planets where available. When only minimum planet mass (i.e., $M\sin i$) and/or minimum eccentricity have been measured (e.g., Kepler 442 where $e > 0.04$, according to Torres et al. 2015), these values have been adopted for mean planet mass (M_P) and e, as in Quick et al. (2020). In cases where planet radius (R_P) or

[7] http://www.pas.rochester.edu/emamajek/EEM_dwarf_UBVIJHK_colors_Teff.txt

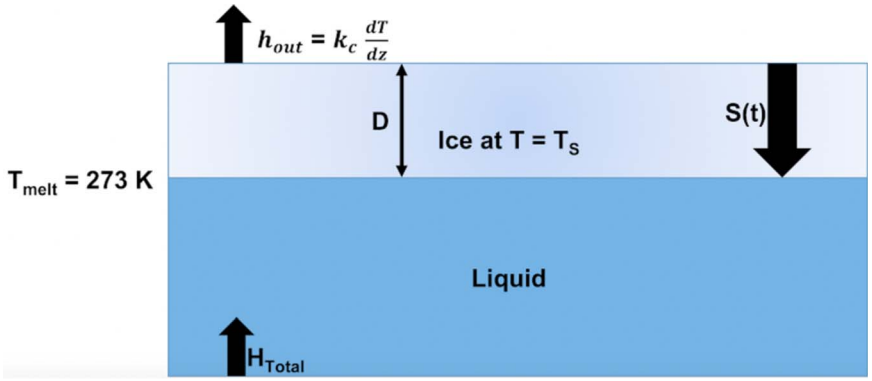

Figure 2. Geometry for the solidification of the subsurface ocean on a cold ocean planet. Here the ice shell is represented as a solid layer at a single, constant surface temperature (T_S), while the subsurface ocean is represented as a layer of liquid. The boundary between the ice shell and ocean has a constant temperature, $T_{\rm melt} = 273$ K. Here $h_{\rm out}$ represents conductive heat loss that causes the solidification front, $S(t)$, to advance. $S(t)$ measures the position of the ice–water interface over time, which defines the instantaneous thickness (D) of the ice shell in response to the gradual cooling of the ocean. $H_{\rm Total}$ represents basal heating added into the system from tidal dissipation and radiogenic sources.

mass are unknown, these parameters were obtained from Figure 4 in Seager et al. (2007), assuming that the planets under consideration are composed of 45% water ice, a 48.5% silicate shell, and a 6.5% iron core akin to large icy ocean moons in our solar system. Planet density (ρ) was then calculated using the relation $\rho = 3M_P/4\pi R_P^3$, and surface gravity (g) was calculated using the relation $g = GM_P/R_P$.

Given observational biases in transit and radial velocity surveys that favor detection of small planets around small stars, many of the planets considered here orbit low-mass M dwarfs. Such stars are on average highly active and have very long pre-main-sequence phases, during which newly formed planets experience higher stellar luminosities (Baraffe et al. 1998, 2002; Khodachenko et al. 2007; Ramirez & Kaltenegger 2014; Bolmont et al. 2017). The first characteristic may negatively affect the ability of orbiting solid planets to retain primordial atmospheres (e.g., Airapetian et al. 2017), while the second may reduce their ability to retain volatiles (e.g., Luger & Barnes 2015). Indeed, it appears that the Earth-sized exoplanet Trappist-1b does not have a substantial atmosphere (Greene et al. 2023). While this planet orbits too close to its host star to have ever been considered a cold ocean planet, other planets in the Trappist-1 system (e.g., f, g, and h) are candidates.

2.1. The Depth to Subsurface Oceans on Cold Ocean Planets

Similar to the case of our solar system's icy moons (Hussmann et al. 2002; Ruiz 2003; Hussmann & Spohn 2004; Roberts & Nimmo 2008; Gaeman et al. 2012; Chen et al. 2014; Quick & Marsh 2015), internal heating due mainly to tidal and radiogenic effects may forestall the freezing of subsurface oceans in cold ocean planets and is likely to significantly contribute to the ongoing evolution of their icy shells and to geological activity at their surfaces. We assume that the external ice shells on cold ocean planets form by the gradual freezing of their oceans from above and employ a Stefan-style solidification solution, which describes the temporal evolution of the phase boundary between two materials that are undergoing a phase change (see Quick & Marsh 2015), to place bounds on the thickness of their icy shells (Figure 2). Hence implicit in the model presented here is that ice shells on cold ocean planets are in a quasi-steady-state, Stefan-style, conductive regime, where outward heat loss is balanced by heating from below due to tidal dissipation and radiogenic heating in their interiors (Figure 2).

In keeping with the steady-state solution, constant radiogenic heating rates have been assumed for each planet, as a function of their age, according to Frank et al. (2014). As in Quick et al. (2020), the age of all planets has been assumed to be commensurate with the approximate age of their host stars, as provided by the references listed in the Table 2 caption. In contrast to previous models that have investigated ice shell thickness on our solar system's ocean worlds (e.g., Hussmann et al. 2002; Hussmann & Spohn 2004), neither the thermal-orbital evolution of these planets nor viscosity variations in their ice shells as manifested by multiple rheological layers, which are poorly constrained for the ocean worlds in our solar system and are unknown for these cold ocean planets, are considered. Indeed, previous modeling has shown that accurate equilibrium ice shell thicknesses are still obtained for ocean worlds when these details are not considered (e.g., see Ruiz 2003; Quick & Marsh 2015). However, unlike previous studies that explored the thicknesses of ice shells on cold ocean planets (e.g., Tajika 2008), the effects of both tidal heating and the changing melting temperature of ice with pressure are considered. In addition, rather than assuming that the amount of water these planets contain, or the amount of radiogenic heating they receive, is equal to that of Earth (e.g., Tajika 2008; Luger et al. 2017), radiogenic heating rates for these worlds are based on their estimated age and size, as in Quick et al. (2020).

As is the case for the icy bodies in our solar system, we envision that liquid water is transported in fractures that extend from the surfaces of these worlds to a global ocean or to discrete pockets of salty water in their interiors (Figure 3). For the case of planets with thin ($\leqslant$10 km) ice shells, cryovolcanic eruptions could be triggered when fractures extending from the base of the ice shell become filled with ocean water and subsequently propagate to the surface (Figure 3(a); Crawford & Stevenson 1988; Fagents et al. 2000; Fagents 2003; Manga & Wang 2007; Matson et al. 2012). Hydrostatic pressure would then cause the water in these fractures to rise 90% of the way to the surface (Matson et al. 2012; Craft et al. 2016), after which the lack of a substantial atmosphere would cause any volatiles contained in the water to separate from the solution. This volatile exsolution triggers explosive cryovolcanic eruptions during which water droplets and icy particles are violently launched on ballistic trajectories (Figure 3(a);

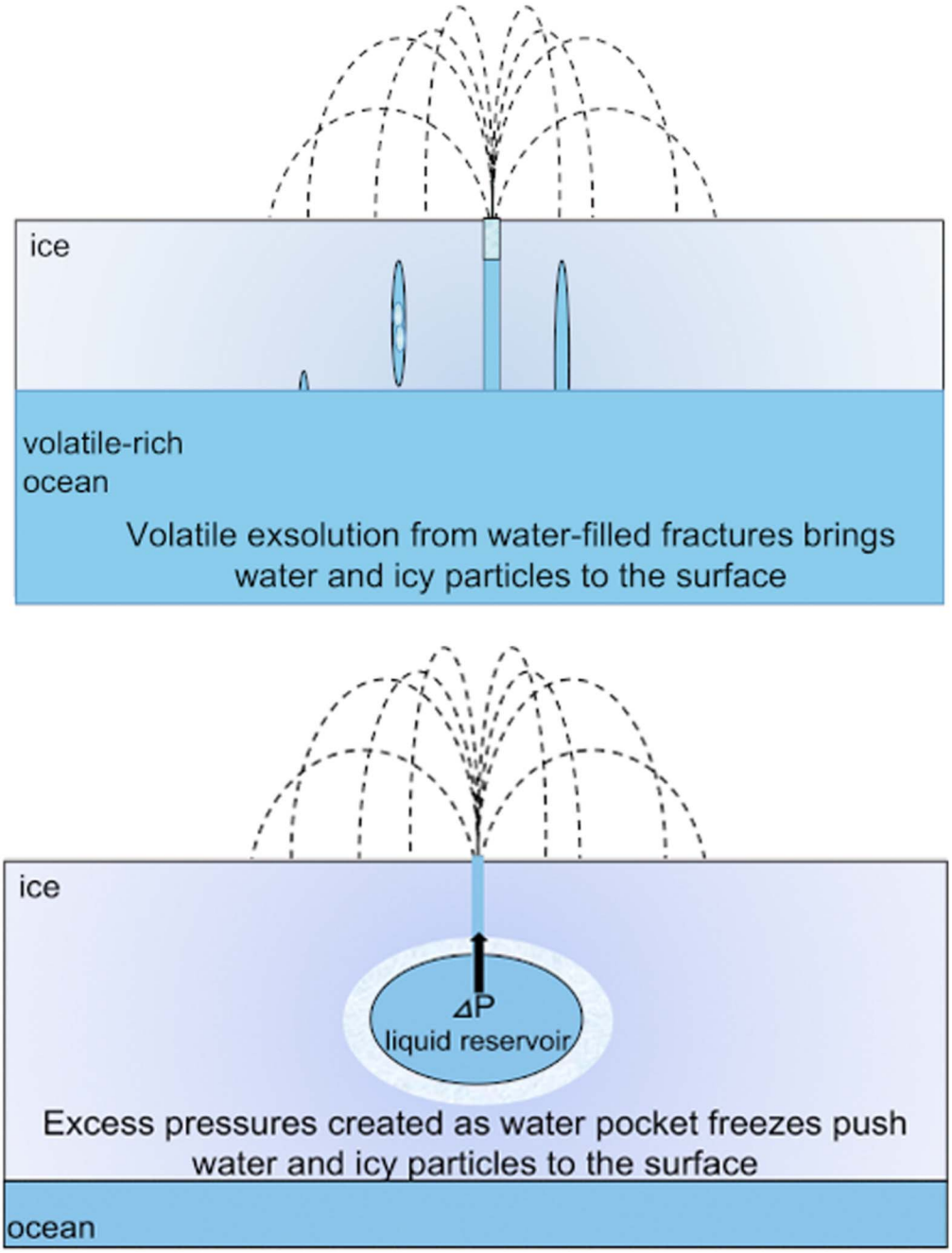

Figure 3. The initiation of cryovolcanism on cold ocean worlds. (a) Cryovolcanism may be initiated on cold ocean planets with thin (approximately <10 km thick) ice shells by the exsolution of volatiles from water-filled fractures connected to a subsurface ocean. (b) Water erupted during explosive cryovolcanic eruptions on cold ocean planets that have relatively thick ice shells, such as OGLE-2005-BLG-390-Lb and Trappist-1h, may be sourced from salty water pockets that are perched in their ice shells, rather than directly from the subsurface oceans. Figures after Fagents (2003).

Crawford & Stevenson 1988; Fagents 2003). Thus, implicit in our models is the assumption that the planets considered here do not have appreciable atmospheres. Under this assumption, the initiation of cryovolcanism via the intersection of water-filled fractures with the surface would be a plausible means of producing cryovolcanic eruptions that bring liquid water to shallow levels.

Conversely, in the presence of thick ice shells, oceans would be located relatively far beneath the surfaces of cold ocean planets. Cryovolcanism would ensue when excess pressures caused by the gradual freezing of crustal fluid reservoirs lead to stress conditions that promote fracturing in their ice shells. Fluids could then be transported to the surface in those fractures, at which time volatile exsolution could trigger explosive cryovolcanism (Figure 3(b); Fagents 2003; Manga & Wang 2007). Thus, the thickness of ice shells on cold ocean planets places fundamental constraints on the proximity of ocean water to the surface and the ease with which cryovolcanism can occur.

While ice shells that are $\geqslant$30 km thick are likely to convect (McKinnon 1999; Roberts & Nimmo 2008; Barr & Showman 2009), convection may be precluded in thick ice shells if their viscosities are $\geqslant 10^{14}$ Pa s or if the water ice that makes up the shell exhibits non-Newtonian behavior (Roberts & Nimmo 2008).

Furthermore, the presence of convective sublayers would be dependent upon any number of unknown properties that vary throughout the ice shell, including viscosity, specific heat, thermal conductivity, porosity, presence and location of clathrates, rheology, and ice grain size (Nimmo et al. 2003; Tobie et al. 2003; Barr & Pappalardo 2005; Levi et al. 2013, 2014; Carnahan et al. 2021; Green et al. 2021). Even in the case of ice shells with basal convecting layers such as Europa and Triton, previous studies have shown that their average total shell thickness can be reliably constrained by assuming that the ice shell is in a purely conductive regime (e.g., Ruiz 2003; Gaeman et al. 2012; Quick & Marsh 2015). Indeed, although heat balance in the ice shell would be altered by the presence of a basal convecting layer, the rate of heat transfer through the ice shell would still be governed by the efficiency of the conductive layer to transmit heat to the surface. Thus, assuming that ice shells on cold ocean planets form in the same manner as the ice shells on the icy moons in our solar system, that is, by freezing of their oceans from the top down (Roberts & Nimmo 2008; Gaeman et al. 2012; Quick & Marsh 2015), the conductive transfer of heat at the thermal boundary layer can be used to accurately estimate ice shell thickness. Given this, and the many unknowns concerning how the onset of convection is affected by both temperature-dependent and mechanical ice shell properties on ocean worlds, inter–ice shell convection has not been considered for the cold ocean planets in this study. This is similar to previous work in which ice shell thicknesses have been obtained for cold ocean planets assuming that ice is in a purely conductive regime (e.g., Tajika 2008).

Previous studies of extrasolar ocean worlds have suggested that, if planets are cold enough to have icy surfaces, illumination from their host stars does not have a major influence on the maintenance of internal oceans and that internal sources of heat from tidal and radiogenic effects are the main factors that influence the depths to liquid layers (Tjoa et al. 2020). Hence, as in Quick et al. (2020), we consider tidal heating and radiogenic heating to be the primary forms of internal heating on cold ocean planets. The total internal heating rate, $H_{\rm Total}$, in a cold ocean planet can therefore be expressed as $H_{\rm Total} = H_{\rm Tidal} + H_{\rm Radiogenic}$ (Quick et al. 2020), where $H_{\rm Tidal} = 21 k_2 \omega^5 R_P^5 e^2 / 2GQ$ (Roberts & Nimmo 2008; Quick & Marsh 2015) and k_2 is the degree 2 Love number, which describes how the planet responds to the tide raised on it by its primary. The value of k_2 ranges from 0 for a completely rigid planet to 1.5 for a planet that is entirely fluid and therefore has a significant tidal response to the gravitational tug of its star. The quantity $\omega \approx 2\pi/P$ is the planet's orbital mean motion, where P is the orbital period, $G = 6.67 \times 10^{-11}$ m^3 kg^{-1}s^{-2} is the gravitational constant, and Q is the quality factor, which represents the fraction of energy that is dissipated as heat within the planet per orbital cycle. A significant amount of tidal energy is dissipated as heat in the interiors of planets that have low Q values. As in Quick et al. (2020), and consistent with past studies of the terrestrial planets and icy moons in our solar system (Kozai 1968; Jackson et al. 2008; Quick & Marsh 2015; Hurford et al. 2020), we have assumed that $k_2 = 0.3$. Commensurate with past studies of tidal dissipation in our solar system's moons (e.g., Cassen et al. 1979; Peale et al. 1979; Chen et al. 2014; Quick & Marsh 2015) and studies that considered moderate amounts of tidal dissipation in terrestrial exoplanets (Henning & Hurford 2014; Tamburo et al. 2018), we adopt $Q = 100$.

Frank et al. (2014) provide radiogenic heating rates per kilogram of mantle mass ($\dot{h}$) for planets as a function of age. Assuming that mantle densities of the cold ocean planets considered here are ~4000 kg m^{-3}, and that these mantles make up 84% of total planet volume as on Earth (Stacey & Davis 2008), total radiogenic heating rates may be obtained using the following relation: $H_{\rm Radiogenic} = 0.84\pi R_P^3\ (16{,}000/3)$ (Quick et al. 2020). We have thus emplaced Earth-like constraints on the relative proportions of mantle mass and volume for each planet. However, previous work has shown that varying the proportion of a planet's mantle volume while employing an Earth-like mantle density produces negligible changes in radiogenic heating estimates (Quick et al. 2020).

If we assume that outward heat loss from a planet is balanced by total internal heating from radiogenic and tidal sources, the thickness of the icy shell on a cold ocean planet (D), and thus the depth to the subsurface ocean beneath the ice shell when the changing melting temperature of ice due to pressure is considered, may be expressed as

$$D = \frac{(273.16 - T_S) k_{\rm ice} 4\pi R_P^2}{H_{\rm Total} + (1.063 \times 10^{-7} \rho_{\rm ice} g k_{\rm ice} 4\pi R_P^2)} \quad (1)$$

(Quick & Marsh 2015). Here T_s, the surface temperature of the planet in question, is assumed to be equal to the planet's average equilibrium temperature (given in Table 1). In cases where the average equilibrium temperature of a cold ocean planet is unknown, it has been obtained using the following expression from Safonova et al. (2016):

$$T_s = \left[\frac{L\ (1 - A)}{16\pi\sigma\varepsilon a^2} \right]^{1/4}, \quad (2)$$

where L is the luminosity of the host star in Watts, A is the planet's bond albedo, $\sigma = 5.67 \times 10^{-8}$ W m^{-2}-K^4 is the Stefan–Boltzmann constant, ε is the emissivity of the planet, and a is the planet's semimajor axis. Here $k_{\rm ice} = 488.19/T_s + 0.486$ is the temperature-dependent thermal conductivity of ice in W/m-K (Hobbs 1974), $\rho_{\rm ice} = 920$ kg m^{-3} is the density of ice, and g is the planet's acceleration due to gravity. Note that although $k_{\rm ice}$ is likely to vary with depth in the ice shells of these worlds, a constant value has been assumed. This ensures minimum insulation, thus preventing underestimation of average ice shell thickness (Quick & Marsh 2015). Previous studies that explored the thicknesses of ice shells on cold ocean planets did not take tidal heating or the changing melting temperature of ice with pressure into account (e.g., Tajika 2008).

2.2. Exosphere Formation and Evaporative Outgassing on Highly Irradiated Cold Ocean Planets

Owing to the relatively close-in orbits of the cold ocean planets in this study (Table 1), their H_2O-rich surfaces would be exposed to high levels of heating and X-ray and extreme ultraviolet (XUV; 1–100 nm) irradiation from their host stars. As a result, these planets would experience extreme volatile loss to space, which could cause very tenuous atmospheres or extended exospheres to form around them. The icy moons in our solar system also have a history of extreme volatile loss. For example, owing to interactions with solar energetic particles and charged particles in Jupiter's magnetosphere, Io, the most volcanically active body in our solar system (Moore 2003; Lopes et al. 2004; McEwen et al. 2004), experiences

extreme volatile loss, including the significant release of volcanically produced SO_2, S, and O to its exosphere (McGrath et al. 2004 and references therein). Conversely, on Europa, where the surface is covered in H_2O ice, volatile loss results in the formation of a surface-bounded, O_2-dominated exosphere on its leading hemisphere and a stable H_2O-dominated exosphere above the trailing hemisphere (Hall et al. 1995, 1998; McGrath et al. 2004; Roth 2021).

Comparisons of the magnitude of volatile loss between Europa and close-in cold ocean planets could therefore be employed to constrain the density of extended exospheres formed by continued XUV irradiation of their surfaces. To estimate whether the evaporative column densities of such exospheres are potentially detectable in transmission spectra, the methods described in Oza et al. (2019) have been employed to perform a basic atmospheric loss calculation for the cold ocean planets listed in Table 1. We explore H_2O mass loss in the energy-limited regime (Watson et al. 1981), since stellar XUV radiation is the main source of surface heating and energy-limited escape has been shown to dominate mass loss for close-in, low-mass planets detected with the Kepler mission (Jin et al. 2014; Fulton & Petigura 2018).

The rate of H_2O mass loss ($\dot{M}_{H_2O}$) from a planet of radius R_P and mass M_P may be approximated as

$$\dot{M}_{H_2O} = \frac{4\pi R_P^2 F_{XUV} m_{H_2O} x_i \eta_{XUV}}{U(R_P)} \quad (3)$$

(Bolmont et al. 2017; Oza et al. 2019), where F_{XUV} is the incident XUV flux on the planet from its host star, $m_{H_2O} = 2.99 \times 10^{-26}$ kg is the mass of one water molecule, and $x_i \sim 1$ is the mass fraction of H_2O in the planet's exosphere. Incident XUV fluxes for each planet as a function of system age and host star spectral type were obtained using the methods of Lammer et al. (2009) with the parameters listed in Table 2. Although the XUV heating efficiency factor (η_{XUV}) strongly depends on the XUV flux (see Bolmont et al. 2017; Bourrier et al. 2017), we assume $\eta_{XUV} = 0.1$, as is typically employed when considering energy-limited escape of water vapor (Yelle 2004; Owen & Wu 2013; Bolmont et al. 2017; Lopez 2017). Finally, $U(R_P) = GM_P m_{H2O}/R_P$ is the gravitational binding energy of a water molecule to the planet. From here, the disk-averaged, line-of-sight (LOS) column density of H_2O stripped from a cold ocean planet to form its exosphere $\langle N_{H_2O} \rangle$ can be expressed as

$$\langle N_{H_2O} \rangle = \frac{\dot{M}_{H_2O} \tau_i}{m_{H_2O} \pi R_*^2} \quad (4)$$

(Oza et al. 2019), where $\tau_i = 4.54 \times 10^7$ sec $(a/a_{Europa})^2$ is the H_2O photoionization time for each planet, scaled to the photoionization time of H_2O on Europa (Shematovich et al. 2005). The parameter a once again represents the planet's semimajor axis, a_{Europa} is Europa's orbital distance from the Sun, and R_* is the radius of the host star as given in Table 2. The results of these calculations represent the LOS column density of evaporating H_2O, and therefore the density of surface bounded exospheres that would be observed in the transmission spectra of the cold ocean planets listed in Table 1 (Oza et al. 2019; Guenther & Kislyakova 2020).

2.3. Cryovolcanic Outgassing on Cold Ocean Planets

Tidally driven explosive cryovolcanic eruptions, in which volatiles would be lofted into space by H_2O-rich geyser-like plumes, may occur on cold ocean planets with nonzero eccentricities (Quick et al. 2020; Kane et al. 2021). As is the case for eruptions on Earth, Europa, and Enceladus, water vapor is likely to be the dominant volatile in volcanic and cryovolcanic eruptions on cold ocean planets (see, Glaze et al. 1997; Hansen et al. 2006; Porco et al. 2006; Spencer et al. 2006; Roth et al. 2014a; Paganini et al. 2020). Europa represents a tidally heated, cold ocean world where cryovolcanism, in the form of geyser-like plumes, has been observed by space- and ground-based telescopes via spectroscopic detections of water vapor and its atomic constituents (Roth et al. 2014b; Sparks et al. 2016, 2017; Paganini et al. 2020). While geysering activity on Enceladus appears to be frequent and continuous (Spencer et al. 2009; Postberg et al. 2018a), Europa's explosive cryovolcanism may be periodic or transient in nature and may display spatial variability (Roth et al. 2014a; Rhoden et al. 2015; Teolis et al. 2017). Furthermore, previous modeling (e.g., Fagents et al. 2000; Quick et al. 2013; Rhoden et al. 2015; Quick & Hedman 2020) and searches for Europa's geyser-like plumes in the Galileo spacecraft data set (Phillips et al. 2000) support the conclusion that Europa's plume activity is sporadic or small scale in nature. Europa therefore represents a conservative baseline for geyser-like activity on a tidally heated ocean world, and the associated activity rates may be utilized to place constraints on the amount of tidally induced cryovolcanism on cold ocean planets.

With this in mind, the magnitude of tidally driven cryovolcanic outgassing rates on cold ocean planets, $\dot{M}_{Volc}$, can be expressed as

$$\dot{M}_{Volc} \cong \left(\frac{\dot{E}_{Tidal}}{\dot{E}_{Tidal_{Europa}}} \right) \dot{M}_{Volc_{Europa}} \quad (5)$$

(Oza et al. 2019), where $\dot{E}_{Tidal}$ and $\dot{E}_{Tidal_{Europa}} = 1 \times 10^{12}$ W (Quick & Marsh 2015; Quick et al. 2020) are the tidal heating rates of a cold ocean planet and Europa, respectively, and $\dot{M}_{Volc_{Europa}} = 2.4 \times 10^3$ kg s^{-1} is the output rate of water vapor from Europa's plumes, that is, the tidally driven cryovolcanic outgassing rate on Europa (Paganini et al. 2020). Cryovolcanic LOS column densities associated with this outgassing, N_{Volc}, may be expressed as

$$N_{Volc} = \left(\frac{\sqrt{H}}{5.7 \pi m_{H_2O} R_P^2 \sqrt{g}} \right) \dot{M}_{Volc} \quad (6)$$

(Oza et al. 2019), where $H = k_b T_{EFF}/m_{H_2O}$ is atmospheric scale height. Here $k_b = 1.38 \times 10^{-23}$ m^{2}kg s^{-2}-K is Boltzmann's constant, T_{EFF} is the planet's effective surface temperature, and $m_{H_2O} = 2.99 \times 10^{-26}$ kg is the mass of one water molecule.

As Equations (3) and (4) can be employed to obtain the XUV-driven evaporating column density of H_2O in transmission spectra, and therefore the density of surface bounded exospheres on these planets (Oza et al. 2019; Guenther & Kislyakova 2020), cryovolcanic outgassing on these planets would be distinguishable as H_2O column densities (Equation (6)) in excess of the evaporative column densities associated with exosphere formation (Guenther & Kislyakova 2020). Such excesses could be

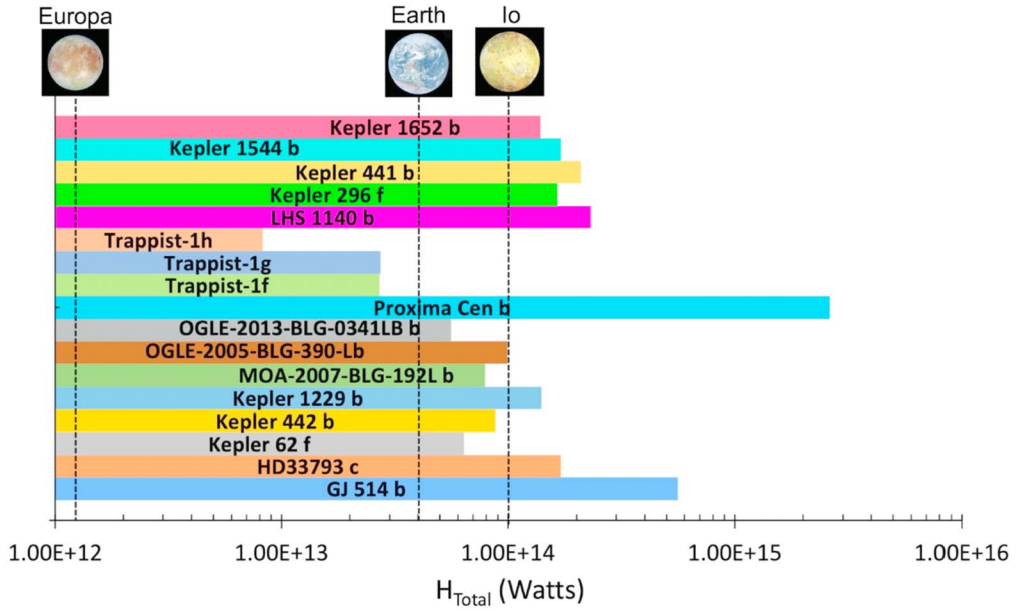

Figure 4. Total internal heating, H_{Total}, for the cold ocean planets in our study compared to H_{Total} for Europa, Earth, and Io. Every planet that we have considered receives more heating from tidal and radiogenic sources than Europa, which is cryovolcanically and tectonically active, and maintains an ocean beneath its icy shell. OGLE 2005-BLG-390-Lb receives approximately the same amount of internal heating as Io, the most volcanically active body in our solar system. Internal heating rates for Kepler 1652 b, Kepler 1544 b, Kepler 441 b, Kepler 296 f, LHS 1140 b, Proxima Cen b, Kepler 1229 b, HD33793 c, and GJ 514 b exceed that of Io. This suggests that all planets in our study receive enough internal heating to maintain internal oceans and cryovolcanic activity at their surfaces. 1 Watt = 10^7 erg s^{-1}.

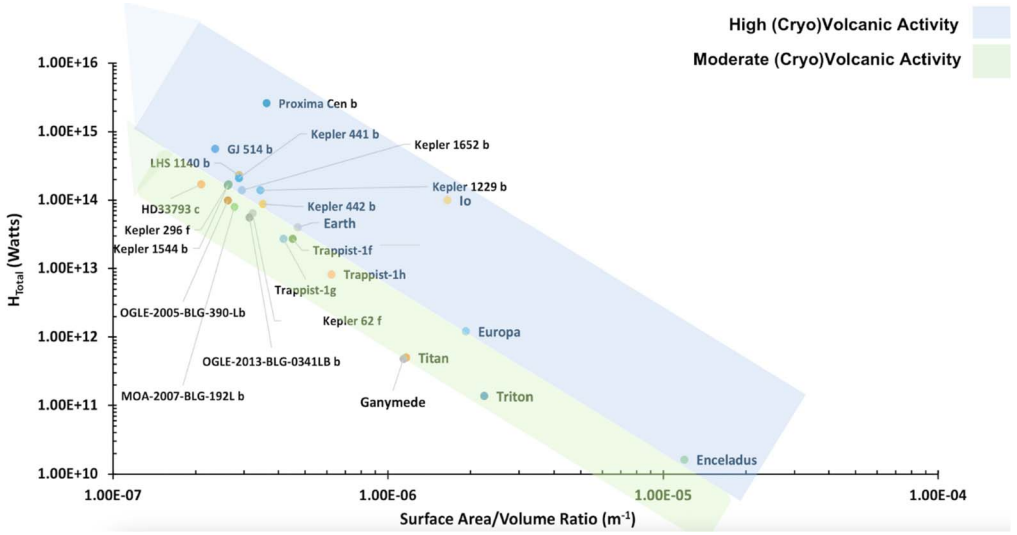

Figure 5. Total internal heating, H_{Total}, for the cold ocean planets in our study compared to H_{Total} for Earth, Io, and the geologically active ocean worlds in our solar system. Compared to volcanic activity rates on Earth and Io, and cryovolcanic activity rates on Europa and Enceladus, all of the cold ocean planets considered here are likely to be cryovolcanically active. Cold ocean planets in the blue shaded region may exhibit very high rates of cryovolcanism with frequent eruptions of large geyser-like plumes that vent water and its constituent molecules into space. Cold ocean planets in the green shaded region are also likely to exhibit cryovolcanism with explosive venting of geyser-like plumes but may have slightly smaller, less frequent eruptions. 1 Watt = 10^7 erg s^{-1}.

used to infer the presence of liquid reservoirs, possibly in the form of internal oceans, and would be indicative of current geological activity on these worlds.

3. Results and Discussion

3.1. Total Internal Heating Rates

Values of H_{Total} for all of the cold ocean planets considered in this study, compared to H_{Total} for several of the volcanically and cryovolcanically active bodies in our solar system, are displayed in Figures 4 and 5. Planets such as MOA-2007-BLG-192Lb and OGLE 2005-BLG-390-L b that have been classified as ice giants in the past (Beaulieu et al. 2006; Bennett et al. 2008) are here assumed to be super Earth-type planets, based on their masses and radii (Table 1). Equilibrium surface temperatures and depths to internal oceans (i.e., ice shell thicknesses) under a variety of conditions, along with tidal and radiogenic heating rates for each cold ocean planet, are shown in Table 3. Differences in heating rates for the outer Trappist planets and LHS 1140 b compared to those reported in Quick et al. (2020) are the result of revised masses for these planets obtained from Agol et al. (2021) and Lillo-Box et al. (2020), respectively.

Table 3
Cold Ocean Planet Surface Temperature and Depth to Ocean Layers as a Function of Planetary Albedo and Emissivity (1 W = 10^7 erg s^{-1})

		Earth-like		Europa-like		Enceladus-like					
		$A = 0.3$, $\varepsilon = 0.85$		$A = 0.55$, $\varepsilon = 0.9$		$A = 0.81$; $\varepsilon \cong 1$					
Planet	[a]Cited T_s (K)	D (km)	T_s (K)	D (km)	T_s (K)	D (km)	T_s (K)	D (km)	$H_{\text{Radiogenic}}$ (W)	H_{Tidal} (W)	H_{Total}(W)
GJ 514 b	202	6.4	182.5	8.7	161	11.9	126.5	18.5	5.6×10^{14}	1.2×10^{12}	5.6×10^{14}
HD33793 c (Kapteyn c)	⋯	⋯	150.5	6.5	132.9	8.2	104.3	12	1.7×10^{14}	1.2×10^{12}	1.7×10^{14}
Kepler 62 f	208	3	224.6	2.1	198	3.6	155.6	6.9	6.4×10^{13}	⋯	6.4×10^{13}
Kepler 296 f	⋯	⋯	213	1.6	188	2.6	147.7	4.6	1.65×10^{14}	4.8×10^{10}	1.65×10^{14}
Kepler 441 b	⋯	⋯	176.8	2	156	2.7	122.5	4.3	$2.1\text{x } 10^{14}$	3.15×10^{9}	$2.1\text{x } 10^{14}$
Kepler 442 b	⋯	⋯	242.8	0.8	214.3	1.7	168.2	3.7	8.8×10^{13}	3.9×10^{9}	8.8×10^{13}
Kepler 1229 b	212	1.2	238.6	0.6	210.6	1.2	165.4	2.5	1.4×10^{14}	⋯	1.4×10^{14}
Kepler 1544 b	269	0.09	249.4	0.5	220.2	1.3	172.9	3.1	1.71×10^{14}	⋯	1.71×10^{14}
Kepler 1652 b	268	0.11	254.2	0.4	224.4	1.2	176.2	2.9	1.4×10^{14}	⋯	1.4×10^{14}
LHS 1140 b	235	0.56	205	1.1	180.7	1.7	141.8	2.9	1.1×10^{14}	1.2×10^{14}	2.3×10^{14}
MOA-2007-BLG-192L b	⋯	⋯	51	34.2	45	38.7	35.4	48.4	7.9×10^{13}	⋯	7.9×10^{13}
OGLE-2005-BLG-390-Lb	50	29.3	48	30.5	42.3	34.2	33.2	42	9.9×10^{13}	⋯	9.9×10^{13}
OGLE-2013-BLG-0341LB b	⋯	⋯	74.3	25.5	65.6	29.4	51.5	38.2	5.6×10^{13}	⋯	5.6×10^{13}
Proxima Cen b	234	0.026	238.8	0.029	210.8	0.058	165.5	0.12	5.7×10^{13}	2.56×10^{15}	2.6×10^{15}
Trappist-1f	219	2.9	237.8	1.8	209.9	3.52	164.8	7.3	2.2×10^{13}	5×10^{12}	2.7×10^{13}
Trappist-1g	198.6	4.8	188	5.75	166	8	130	12.9	2.7×10^{13}	2.8×10^{11}	2.8×10^{13}
Trappist-1h	168	11.8	163.5	12.6	144	16.4	113	24.7	8.2×10^{12}	3.4×10^{10}	8.2×10^{12}

Note.
[a] Cited T_S is the average equilibrium temperature for these planets as cited in Beaulieu et al. (2006), Borucki et al. (2013), Anglada-Escudé et al. (2016), Torres et al. (2017), Gillon et al. (2017), Damasso et al. (2022). In all cases, Equation (1) has been employed to constrain depth to the ocean layer (i.e., ice shell thickness), D.

Total internal heating rates for Io, Europa, Enceladus, and Earth are 1×10^{14}, 1.2×10^{12}, 1.6×10^{10}, and 4.7×10^{13} W, respectively (Quick et al. 2020). Figures 4 and 5 illustrate that when compared with these worlds, H_{Total} values for all the cold ocean planets considered in our study are high enough for them to maintain internal oceans and to be cryovolcanically active. Cryovolcanic activity rates on GJ 514 b, Kepler 442 b, Kepler 1229 b, Kepler 1544 b, Kepler 1652 b, LHS 1140 b, and Proxima Cen b may be very similar to Io's volcanic activity rates (Figures 4 and 5). Indeed, these planets may exhibit very high rates of cryovolcanism in the form of geyser-like plumes, effusive cryolava flows at their surfaces, and cryomagmatism in the form of diapiric upwellings and convection in their interiors. Based on their values for H_{Total}, the remainder of the planets in our study are also likely to experience cryovolcanic activity and cryomagmatism, albeit at slightly lower rates—somewhat larger than on Europa and more similar to volcanic activity rates on Earth (Figure 4). We hasten to add that despite estimates for high internal heating rates, all of these worlds are likely to be icy, cryovolcanic worlds rather than lava worlds. Despite its high volcanic activity levels, Io, which has a density of approximately 3527 kg m^{-3} (Schubert et al. 2004) and a maximum surface temperature of 130 K (Rathbun et al. 2004), is an icy moon. Indeed, Io's surface is covered in SO_2 frost with localized patches of water ice and traces of H_2O and H_2S frozen into SO_2ice (McEwen et al. 2004).

3.2. Cold Ocean Planet Surface Temperatures and Depths to Subsurface Oceans

In the case of cold ocean planets with equilibrium surface temperatures previously cited in the literature, all, with the exception of OGLE-2005-BLG-390-Lb, may have fairly thin ice shells. Oceans on these planets would be located fairly close to their surfaces, as is the case for Enceladus, where the ocean is located $\leqslant$10 km beneath the south polar surface (Iess et al. 2014; Hemingway et al. 2018). Proxima Cen b, Kepler 1544 b, and Kepler 1652 b are especially notable, as oceans on these planets would lie less than ~100 m beneath their surfaces. Such thin ice shells suggest that cryovolcanic eruptions would be sourced directly from their oceans as they are on Enceladus (Manga & Wang 2007; Postberg et al. 2009, 2011; Hsu 2015; Thomas et al. 2016; Postberg et al. 2018). However, OGLE-2005-BLG-390-Lb would have an ice shell that is almost 30 km thick (Table 3). Similar to Europa, which has an ice shell with an average thickness of 25–30 km (McKinnon 1999; Hussmann et al. 2002; Quick & Marsh 2015), cryovolcanic eruptions on OGLE-2005-BLG-390-Lb may not be sourced directly from a subsurface ocean. Rather, eruptions might be sourced from pressurized water pockets perched within the icy shell (Figure 3(a); see Fagents 2003; Manga & Wang 2007; Schmidt et al. 2011; Manga & Michaut 2017).

Notwithstanding, it is important to note that employing Equation (1) while utilizing the estimated equilibrium surface temperatures found in the literature (Table 1) will result in underestimates of ice shell thicknesses, as in many cases bond albedos that are not characteristic of planets with icy or liquid water surfaces have previously been assumed. For example, the cited equilibrium surface temperatures of 219, 198.6, and 168 K for Trappist-1f, g, and h, respectively, were obtained assuming a "null" bond albedo (Gillon et al. 2017), and the 208 K equilibrium surface temperature for Kepler 62 f was obtained by assuming that plausible bond albedos for the planet

Table 4
Planets Unlikely to Be Habitable

Planet	Assuming Earth-like Albedo and Emissivity $A = 0.3$, $\varepsilon = 0.85$ T_s (K)	Assuming Europa-like Albedo and Emissivity $A = 0.55$, $\varepsilon = 0.9$ T_s (K)	Assuming Enceladus-like Albedo and Emissivity $A = 0.81$; $\varepsilon \cong 1$ T_s (K)
Kepler 11 b	943	832	654
Kepler 18 b	1133	1000	785
Kepler 60 b	1199	1058	831
Kepler 60 c	1156	1020	801
Kepler 60 d	1011	892	701
Kepler 414 b	1049	926	727

are between 0 and 0.5 (Borucki et al. 2013). The 235 K equilibrium surface temperature obtained for LHS 1140 b in Ment et al. (2019) assumed a bond albedo of 0, while Lillo-Box et al. (2020) derived a 378.9 K equilibrium surface temperature for the same planet assuming pressure and temperature conditions equal to those on Earth. Additionally, the 234 K blackbody equilibrium temperature that has been cited for Proxima Cen b (Anglada-Escudé et al. 2016) translates to an albedo of 0. For these reasons, it is necessary to explore plausible equilibrium surface temperatures utilizing the thermophysical properties of ocean worlds in our solar system as baselines (Table 3). Thus, Equations (1) and (2) have been employed to obtain surface temperatures and ice shell thicknesses for each planet considering surface albedos and emissivities that are consistent with Earth ($A = 0.3$, $\varepsilon = 0.85$), Europa ($A = 0.55$, $\varepsilon = 0.9$; Spencer et al. 1999; Abramov & Spencer 2008), and Enceladus ($A = 0.81$; $\varepsilon \cong 1$; Abramov & Spencer 2009; Howett et al. 2010) (Table 4).

In most cases, the equilibrium surface temperatures that were obtained by applying Earth-like thermophysical properties in Equation (2) were slightly colder than or approximately equal to the equilibrium surface temperatures previously reported in the literature (Table 3). Corresponding depths to ocean layers (i.e., ice shell thicknesses) are fairly close to those that would be obtained using previously cited equilibrium surface temperatures in Equation (1), with a few exceptions. The equilibrium surface temperatures obtained using Equation (2) for Kepler 1554 b and 1652 b are ∼20 and 14 K lower than the equilibrium surface temperatures cited in the literature, respectively. As a result, estimated ice shell thicknesses for these planets increased significantly, from 90 to 500 m for Kepler 1544 b and from 110 m to 400 m for Kepler 1652 b (Table 3). Conversely, for Kepler 62 f, Proxima Cen b, and Trappist-1f, newly calculated equilibrium surface temperatures are ∼5 to 19 K warmer than those previously cited in the literature. Corresponding depths to ocean layers decreased on all of these worlds. For example, an ocean on Proxima Cen b would be 4 m closer to its surface (Table 4). Table 4 shows that even when assuming Earth-like thermophysical properties, all planets in this study would still have equilibrium surface temperatures <255 K. Indeed, the highest equilibrium surface temperature obtained assuming Earth-like thermophysical properties is 254 K for Kepler 1652 b (Table 3).

Equilibrium temperatures and ice shell thicknesses obtained using Europa-like thermophysical properties are up to 49° lower (e.g., Kepler 1544 b) and ∼5 km thicker, respectively (e.g., GJ 514 b, Trappist-1h), than those obtained using equilibrium surface temperatures cited in previous literature (Table 4). Assuming thermophysical properties identical to Europa, MOA-2007-BLG-192L b, OGLE-2005-BLG-390-Lb, and OGLE-2013-BLG-0341LB b have very low equilibrium surface temperatures of approximately 45, 42, and 66 K, respectively, and their oceans may lie relatively far beneath their surfaces at depths of approximately 39, 34, and 29 km, respectively (Table 3). Owing to their very thick ice shells, any cryovolcanic eruptions on these worlds would likely be sourced from discrete water pockets that are perched within their ice shells instead of directly from their oceans (Figure 3).

Assuming that the cold ocean planets in our study have Enceladus-like thermophysical properties returns even lower estimated equilibrium surface temperatures and by extension much greater ice shell thicknesses for each planet. For example, depths to oceans on several planets, including GJ 514 b, Kepler 1229 b, Proxima Cen b, and the Trappist planets, are ∼2–3 times larger when considering albedos and emissivities identical to those of Enceladus, while oceans lie at depths that are ∼4 and 6 times larger for Kepler 1652 b and Kepler 1544 b, respectively. Moreover, equilibrium surface temperatures for Kepler 1652 b and Kepler 1544 b are almost 100° lower than when considering equilibrium surface temperatures from the literature (Table 3). Assuming an albedo and emissivity identical to that of Enceladus for Trappist-1f and g results in oceans layers that are ∼7 and 13 km beneath the ice. Equilibrium surface temperatures are even lower and ice shells are even thicker for MOA-2007-BLG-192L b, OGLE-2005-BLG-390-Lb, and OGLE-2013-BLG-0341LB b when an Enceladus-like albedo and emissivity are considered. Equilibrium surface temperatures are approximately 35, 33, and 52 K for these worlds, while their oceans would lie ∼48, 42, and 38 km, beneath their icy surfaces, respectively.

Assuming a geothermal heat flux identical to Earth's, Luger et al. (2017) noted that an ocean may exist beneath 2.8 km of surface ice on Trappist-1h. However, Table 2 shows that radiogenic heating on Trappist-1h is likely to be less than Earth's by almost a factor of 5. Employing Equation (1) while considering a geothermal heat flux that is a function of Trappist-1h's mantle mass and system age (see Frank et al. 2014) and including heating from tidal sources returns ice shell thicknesses that are much greater than 2.8 km under all albedo and emissivity assumptions considered here. Indeed, the depth to an ocean layer on Trappist-1h assuming a null bond albedo, as in Gillon et al. (2017), would be approximately 12 km, while oceans would be located ∼16 to 25 km beneath Trappist-1h's surface if thermophysical properties identical to Europa and Enceladus were assumed (Table 3).

Conversely, for all albedo scenarios considered here, ocean layers on Kepler 296 f, Kepler 441 b, and Kepler 442 b would lie <5 km beneath their surfaces; oceans on Kepler 1229 b, Kepler 1544 b, Kepler 1652 b, and LHS 1140 b would be located ⩽3 km beneath their surfaces; and Proxima Cen b's

ocean would lie less than 100 m beneath its surface. If these worlds are indeed cryovolcanically active, it is very likely that oceanic constituents would be vented directly into space during explosive cryovolcanic eruptions, as is the case for Enceladus (Postberg et al. 2009, 2011; Hsu 2015; Thomas et al. 2016; Postberg et al. 2018). This could also be the case for Trappist-1h, if its ice shell were only 12 km thick. However, assuming an icy surface for this planet and higher associated bond albedos, it is likely that any ocean layer would be 16–24 km beneath Trappist-1h's surface. Thus, any fluids vented into space during explosive cryovolcanic eruptions would most likely issue from salty water pockets in its ice shell.

Oceans would lie even farther beneath the surfaces of MOA-2007-BLG-192L b, OGLE-2005-BLG-390-Lb, and OGLE-2013-BLG-0341LB b (Table 3), and cryovolcanic eruptions on these worlds would also issue from pressured water pockets in their ice shells. We note that consideration of convection within cold ocean planet ice shells could result in much thinner ice shell estimates (see Green et al. 2021) and oceans located closer to their surfaces. Thus, depending on the thermomechanical properties of the ice shells on each planet, ice shell thicknesses and depths to ocean layers reported here may represent upper bounds. As ice shell thermomechanical properties are generally poorly constrained for the ocean worlds in our solar system, we have made no attempt to estimate them for the planets in this study.

Employing Equation (2) to constrain equilibrium surface temperatures for several Kepler planets that were deemed cold ocean planets, ocean planets, or candidate ocean planets in Quick et al. (2020) revealed that some of them, namely, Kepler 60 b, Kepler 60 c, Kepler 60 d, Kepler 11 b, and Kepler 414 b, are likely far too warm for water to exist on their surfaces, either in liquid form or as ice (Table 3). Hence the number of suspected ocean planets in Quick et al. (2020) may be 9/53 instead of 14/53, representing a decrease in the percentage of ocean planets reported in that study from ∼26% to ∼17%. Furthermore, we find that Kepler 18 b, on which water vapor and water clouds have been detected and which has been considered potentially habitable (Cloutier et al. 2017; Benneke 2019; Tsiaras et al. 2019), may be too warm for liquid water to exist at the surface. Based on their equilibrium surface temperatures (Table 4) and estimates provided for their internal heating rates in Table 1 of Quick et al. (2020), all of these planets, including Kepler 18 b, for which $H_{\rm Total} = H_{\rm Radiogenic} = 1.3 \times 10^{14}$ W (according to Cochran et al. 2011, $e = 0$ for Kepler 18 b so $H_{\rm Tidal} = 0$), are likely to be Super-Ios (SI)or Magma Ocean Worlds (MOWs) according to the proposed classification schemes in Quick et al. (2020).

Equation (4) of Oza et al. (2019) may be used to explore equilibrium surface temperatures for cold ocean planets when contributions from tidal heating are included. Employing their Equation (4) for Proxima Cen b, the cold ocean planet in our study that experiences the most tidal heating, raises the range of equilibrium temperatures from ∼166–239 to 251–324 K depending on the bond albedo and emissivity assumed. This suggests that Proxima Cen b could still have an icy surface, perhaps with transient pools of liquid water or "slush" in regions of the planet where tidal heating is concentrated. This is consistent with past work suggesting that, despite Proxima Cen's high levels of stellar activity, Proxima Cen b is likely to have retained significant amounts of water (Ribas et al. 2016) and that its surface may be partially or entirely covered with ice, global or regional oceans, lakes, or a combination of these (Turbet et al. 2016; Del Genio et al. 2019). We note that tidally locked planets with nonzero eccentricities will not be in synchronous rotation; therefore, any planets with significant tidal heating will not have permanent day/night sides.

Employing Equation (4) of Oza et al. (2019) for LHS 1140 b results in temperatures that range from 177 to 270 K when tidal heating is considered. In addition, maximum equilibrium surface temperatures of 246 and 258 K are obtained for Kepler 442 b and Trappist-1f, respectively, when an Earth-like albedo and emissivity are assumed. Thus, even in the absence of appreciable atmospheres, pools of liquid water or regional oceans may also exist on these planets in localized areas where tidal heating is concentrated. While contributions from tidal heating would cause surface temperature increases in the remainder of the planets in our study for which eccentricities are known and are nonzero, we find that these contributions alone would not increase their equilibrium temperatures enough to allow for liquid water rather than ice at their surfaces under any of the circumstances considered here. We note, however, that in the absence of tidal heating, Kepler 1544 b and Kepler 1652 b would have equilibrium surface temperatures of 249 and 254 K, respectively, assuming Earth-like thermophysical properties. Conditions on these planets could therefore be similar to those described for the planets above, with pools of liquid water or slush dotting the surface.

It must be emphasized that while Equation (1) has been employed to obtain average equilibrium ice shell thicknesses for the planets in this study based on their equilibrium surface temperatures, variations in ice shell thickness and depths to ocean layers may be common, as is the case for the icy moons in our solar system. For example, while Europa's average surface temperature is ∼100 K, temperatures at its poles are ∼50 K (Ojakangas & Stevenson 1989). Hence while the average thickness of Europa's ice shell is ∼30 km, it may be as thick as ∼66 km at the poles (Quick & Marsh 2015). Notwithstanding, even Europa's polar ice shell may be locally thin or experience localized melting in areas where tidal heating is concentrated (e.g., Greenberg et al. 1999; O'Brien et al. 2002; Sotin et al. 2002; Schmidt et al. 2011; Quick & Marsh 2015). Furthermore, although Enceladus's ice shell is on average 25 km thick owing to its ∼70–80 K average surface temperature (e.g., Roberts & Nimmo 2008; Bland et al. 2012; Nimmo et al. 2018), it is approximately 14 km thick at the north pole and ⩽10 km thick at the cryovolcanically active south pole, where temperatures may locally exceed 157 K (e.g., Spencer et al. 2006; Abramov & Spencer 2009; Iess et al. 2014; Thomas et al. 2016; Le Gall et al. 2017). Tidal heating, which is concentrated at the poles, serves to thin the ice shell at those locations (Nimmo 2020). Similarly, local variations in ice shell thickness and melt-through may exist for all of the cold ocean planets that were considered in our study, especially those that are subject to high levels of tidal heating from their host stars. Interestingly, there are no conditions under which these planets would be expected to have Ganymede-, Callisto-, or Titan-like ice shells >100 km thick. Rather, they all fall into the Europa/Enceladus regime with average equilbirium ice shell thicknesses <50 km (Table 3). Indeed the large radii, combined, in several cases with relatively high surface temperatures (i.e., estimated equilibirum surface temperatures ≥∼200 K in some

Table 5
Column Densities and Outgassing Rates for Cold Ocean Planets Assuming that Their Atmospheres/Exospheres Are Dominated by H_2O and/or that H_2O Is Their Primary Cryovolcanic Volatile, as on Jupiter's Moon Europa

Planet	$\dot{M}_{H_2O}$ (kg s^{-1})	$\langle N_{H_2O}\rangle$ (molecules m^{-2})	$\langle N_{O_2}\rangle$ (molecules m^{-2})	$\dot{M}_{Volc}$ (kg s^{-1})	N_{Volc} (molecules m^{-2})
GJ 514 b	2.5×10^4	6.5×10^{17}	5.7×10^{17}	2.9×10^3	2.5×10^{15}
HD33793 c (Kapteyn c)	1.3×10^3	5.4×10^{16}	4.8×10^{16}	2.8×10^3	1.7×10^{15}
Kepler 62 f	717	2.54×10^{16}	2.23×10^{16}	⋯	⋯
Kepler 296 f	9.3×10^3	1.22×10^{17}	9.2×10^{16}	115	1.6×10^{14}
Kepler 441 b	9.2×10^3	4.6×10^{17}	3.6×10^{17}	7.5	1.3×10^{13}
Kepler 442 b	1.3×10^4	2.2×10^{17}	$1{,}95 \times 10^{17}$	9.4	3.4×10^{13}
Kepler 1229 b	2.4×10^4	2.4×10^{17}	2.1×10^{17}	⋯	⋯
Kepler 1544 b	3.2×10^3	7.9×10^{16}	6.3×10^{16}	⋯	⋯
Kepler 1652 b	3.4×10^4	2.3×10^{17}	1.8×10^{17}	⋯	⋯
LHS 1140 b	1.9×10^4	1.4×10^{17}	1.2×10^{17}	2.9×10^5	2.9×10^{17}
MOA-2007-BLG-192L b	370	4.1×10^{17}	3.6×10^{17}	⋯	⋯
OGLE-2005-BLG-390-Lb	21.4	2×10^{16}	1.8×10^{16}	⋯	⋯
OGLE-2013-BLG-0341LB b	333	1.7×10^{17}	1.5×10^{17}	⋯	⋯
Proxima Cen b	2.1×10^5	9×10^{17}	7.9×10^{17}	6.1×10^6	2×10^{19}
Trappist-1f	1.7×10^5	3.7×10^{17}	3.3×10^{17}	1.2×10^4	5.1×10^{16}
Trappist-1g	6.5×10^4	3.7×10^{17}	3.2×10^{17}	672	2.1×10^{15}
Trappist-1h	4.5×10^4	4.5×10^{17}	3.9×10^{17}	82	7.2×10^{14}

Note. $\dot{M}_{Volc} = 2 \times 10^3$ kg s^{-1} and $N_{Volc} = 10^{19}$ molecules m^{-2} for Europa (Paganini et al. 2020; Roth 2021).

cases), would preclude thicker ice shells from forming on the cold ocean planets considered here.

3.3. Exosphere Formation and Cryovolcanic Outgassing

Roth (2021) reports LOS column densities for the H_2O exosphere on Europa's trailing hemisphere of $\sim 3 \times 10^{19}$ molecules m^{-2}. Table 5 shows that exosphere column densities of H_2O ($\langle N_{H_2O}\rangle$) for most of the planets considered in our study would be ∼2–3 orders of magnitude less than this (Table 5). However, predicted H_2O column densities for exospheres on Proxima Cen b and GJ 514 b are within an order of magnitude of that on Europa's trailing hemisphere, and predicted exosphere column densities of O_2 ($\langle N_{O_2}\rangle$) are on par with column densities for the O_2-dominated portion of Europa's exosphere (10^{18}–10^{19} molecules m^{-2}; McGrath et al. 2004 and references therein; Roth 2021). These planets may therefore have exospheres that resemble Europa's. However, as column densities in substantial collisional atmospheres typically are $\geqslant 10^{20}$–10^{21} molecules m^{-2}, (Stern 1999; Lellouch et al. 2015), the amount of H_2O lost from the highly irradiated surfaces of these cold ocean planets would not be sufficient to produce substantial atmospheres. The results presented here suggest that even if these planets are not cryovolcanically active, heating owing to their close-in orbits could still lead to evaporation of their surfaces and subsequent outgassing but that without abundant cryovolcanism, most of the planets in this study would have exospheres similar to those of Mercury and the Moon rather than Io-like collisional atmospheres (e.g., Stern 1999; Oza et al. 2019; and references therein).

Estimated tidally driven cryovolcanic outgassing rates ($\dot{M}_{Volc}$) and tidally driven cryovolcanic column densities of water vapor (N_{Volc}) for the planets considered in this study are also displayed in Table 5. Here it has been assumed that eruptions are driven by tidal heating from each of the planet's respective host stars, and atmospheric scale height (H) in Equation (6) has been obtained by employing values for T_{EFF} that are consistent with Europa-like albedos and emissivities (see Table 4). Note that $\dot{M}_{Volc}$ and N_{Volc} have only been calculated for the cold ocean planets whose eccentricities are known (Table 1).

The output of water vapor from Europa's geyser-like plumes is 2.4×10^3 kg s^{-1} (Paganini et al. 2020). The estimated water vapor output ($\dot{M}_{Volc}$) from tidally driven cryovolcanic eruptions on LHS 1140 b, Proxima Cen b, and Trappist-1f far exceeds this value (Table 5), while the amount of water vapor released during geyser-like eruptions on GJ 514 b and HD33793 c would be very similar to the amount of water vapor released during explosive cryovolcanic venting on Europa. Conversely, despite having higher total internal heating rates compared to Europa (Figure 4), tidal heating rates on Trappist-1g, Trappist-1h, Kepler 296 f, Keppler 441 b, and Kepler 442 b are several orders of magnitude lower than the 1×10^{12} W of tidal heating that Europa experiences. Indeed, the proportion of internal heating supplied to these planets by radiogenic sources is several orders of magnitude greater than that supplied by tidal heating from their host stars (Table 4). Thus, tidally driven cryovolcanic venting on these worlds would be more subdued than on Europa, with water vapor outputs for the two outer Trappist planets and Kepler 296 f being 1–2 orders of magnitude lower than Europa's and outputs on Kepler 441 b and Kepler 442 b being the lowest of all at 7.5 and 9.4 kg s^{-1}, respectively (Table 5). It must be noted that although the estimated amount of water vapor that would be outgassed during tidally driven cryovolcanic eruptions on LHS 1140 b, Proxima Cen b, and Trappist-1f is far greater than the water vapor outgassed during explosive cryovolcanism on Europa, it would still be too meager to form collisional atmospheres on these planets, as estimated column densities are $<10^{20}$–10^{21} molecules m^{-2} (Table 5).

Given the expectation that the cold ocean planets considered here will lack collisional atmospheres, the question of how cryovolcanic activity might be detected is challenging to answer. Notwithstanding, possible observational techniques that could be employed to detect water vapor absorption features include: (1) transmission spectroscopy of transiting planets, (2) eclipse spectroscopy of transiting planets, and (3) high-contrast reflectance spectra of directly imaged planets.

The time variability of water vapor abundances produced by cryovolcanic outgassing could prove an advantage for detection by allowing differential measurements. However, while detailed feasibility calculations have not yet been done, the relatively low H_2O column densities produced by cryovolcanic outgassing (Table 5) suggest that detecting cryovolcanic activity by employing these techniques could prove to be quite difficult.

A fourth option would be to look for indirect signs of cryovolcanism rather than explicit detections of water vapor. For example, an anomalously high albedo could suggest a planet that has been freshly resurfaced with water ice from active cryovolcanism, as in the case of Enceladus, which has a bond albedo of 0.81 (Howett et al. 2010) and a geometric albedo >1 (i.e., Enceladus' geometric albedo is 1.38 according to Verbischer et al. 2007). Other features of a planet's reflectance spectrum might be called upon to support this conclusion, such as a moderately blue continuum in the visible through near-IR as shown by Enceladus (Hendrix & Hansen 2010) and solid-state ice absorption features. All of these cryovolcanic activity signs would hinge upon obtaining a direct reflectance spectrum of the planet, and therefore would require the planet to be outside of the inner working angle of a coronagraph or starshade.

The column density of H_2O in recent detections of cryovolcanic venting on Europa with the Keck Observatory is on the order of 10^{19} molecules m^{-2} (Paganini et al. 2020). While the column densities of cryovolcanically outgassed H_2O (N_{Volc}) on the majority of the planets considered in this study would be much smaller by several orders of magnitude, the estimated column density of cryovolcanically outgassed H_2O on Proxima Cen b would be very similar to this value (Table 5). At first glance, Proxima Cen b would appear to be the best candidate for detection of cryovolcanism on an exoplanet using next-generation space- and/or ground-based telescopes. Unfortunately, Proxima Cen b does not transit, ruling out detection of time-variable H_2O excesses in transmission spectra. In addition, the planet is very challenging for a future space-based direct spectroscopy mission like Habitable Worlds Observatory, as it orbits very close to its host star (0.04864 au = 37.″36) and is likely to be interior to the inner working angle of a future coronagraph instrument. The most promising opportunity to search for cryovolcanic activity from Proxima Cen b may come with direct spectroscopy instruments on the future ground-based Extremely Large Telescopes (ELTs) ; their reduced contrast performance but very small inner working angles should make them well-suited to direct observations of exoplanets around low-mass stars.

The estimated amount of water vapor released during episodes of tidally driven cryovolcanism on LHS 1140 b would be larger than the amount of water vapor released into its exosphere by more than a factor of 2 (Table 5). Thus, cryovolcanic outgassing of water vapor on LHS 1140 b might also be telescopically detected. For the remainder of the cold ocean planets in this study, evaporative column densities resulting from the stripping of H_2O from their surfaces and the formation of their exospheres would exceed H_2O column densities that would be vented during tidally driven cryovolcanic eruptions by several orders of magnitude (Table 5). It could therefore be difficult to identify explosive cryovolcanism in the spectra of these planets. Nevertheless, cryovolcanic outgassing may still be distinguishable as H_2O column densities that are in excess of the evaporative column densities associated with exosphere formation, especially in cases where these excesses appear at regular intervals.

Here it has been assumed that H_2O serves as the primary cryovolcanic volatile and exospheric constituent on these worlds. However, the estimates provided above can be reformulated for other volatiles such as O_2, CO_2, CH_4, and so on, which may play major roles in explosive cryovolcanic eruptions and exosphere formation on cold ocean planets. Unlike the case of Europa, in which the exosphere is dominated by H_2O only on its trailing hemisphere, we have assumed that H_2O is the globally dominant exospheric species for all of the planets considered here. However, as both the molecular masses and photoionization times at Europa for H_2O and O_2 are similar, estimated column densities for H_2O-dominated and O_2-dominated exospheres obtained from Equation (2) would be similar. Indeed, the results presented in Table 5 indicate that the column densities of H_2O released during cryovolcanic eruptions on Proxima Cen b and LHS 1140 b would be almost identical to the amount of O_2 that would be present in an O_2-dominated exosphere.

We also hasten to add that the results presented here constrain rates of cryovolcanic outgassing, assuming that tidal heating from the host star is the main facilitator of explosive eruptions on these worlds. However, Table 4 shows that in several instances, internal heating from radiogenic sources exceeds that produced by tidal heating by several orders of magnitude. Indeed, radiogenic heating is a greater contributor to the total internal heating of GJ 514 b, HD33793 c, Kepler 296 f, Kepler 441 b, Kepler 442 b, and Trappist-1f, g, and h. Figures 4 and 5 also illustrate that when radiogenic heating rates are considered for all of these planets, their total internal heating rates are indicative of geological activity at their surfaces that rival levels on Earth, if not Io, which is the most volcanically active body in our solar system (Lopes et al. 2004; McEwen et al. 2004). Induction heating may also contribute to the total internal heating of, and thus aid in facilitating cryovolcanism on, all of the planets considered here, which orbit fairly close to their host stars (see Kislyakova et al. 2017, 2018; Guenther & Kislyakova 2020). Induction heating may have played a major role in the outgassing and internal heating of Proxima Cen b early in its evolution (Noack et al. 2021) and may significantly contribute to the internal heat budgets of planets in young systems where stellar magnetic fields are strongest, such as GJ 514 b, Kepler 441 b, Kepler 442 b, and Kepler 1229 b. Finally, while we have considered tidal heating by solid bodies tides, additional heating caused by obliquity tides in subsurface oceans of these worlds may also contribute, as it does for Neptune's icy ocean moon, Triton (see Chen et al. 2014; Millholland & Laughlin 2019). Hence, when taking additional heating sources into consideration, it is possible that the amount of H_2O outgassed during cryovolcanic venting on all of these worlds may be high enough that water vapor excesses due to cryovolcanism could be telescopically detected.

This study has not accounted for atmospheric effects on the planets considered here. It has been assumed that a lack of substantial atmospheres on these worlds would both ensure that their equilibrium surface temperatures remain below 255 K and facilitate the detection of H_2O-dominated cryovolcanic venting from their surfaces. However, it must be noted that MOA-2007-BLG-192L b may have an atmosphere dominated by N_2 or CO_2,

while OGLE 2005-BLG-390-L b's wide orbit may allow for the retention of substantial primordial H_2 and He in an atmosphere (Pierrehumbert & Gaidos 2011). Furthermore, Trappist-1f and g may have O_2-, CO_2-, or CO_2–O_2-dominated atmospheres (Barth et al. 2021; Krissansen-Totton & Fortney 2022), while Proxima Cen b could have an appreciable atmosphere dominated by CO_2, N_2, or O_2 (Ribas et al. 2016; Turbet et al. 2016; Snellen et al. 2017). We note, however, that at temperatures consistent with MOA-2007-BLG-192L b's equilibrium surface temperature, N_2 and CO_2would be frozen. CO_2 is also normally frozen at the minimum surface temperatures explored for Trappist-1f and g and Proxima Cen b (Table 4). Hence, atmospheres dominated by these species could undergo deposition at the planets' surfaces.

4. Conclusions

All of the planets considered in this study are large enough and experience enough internal heating for them to contain subsurface oceans at varying depths beneath external ice shells and for them to host active geological processes, notably cryovolcanism. If experience with the ocean worlds in our solar system is any indicator, the thin ice shells we have estimated for Proxima Cen b, Trappist-1f, and all of the Kepler planets in our study suggest that any eruption products vented into space during episodes of explosive cryovolcanism on these worlds would issue directly from their subsurface oceans. This may also be the case for GJ 514 b, HD33793 c (Kapteyn c), and Trappist-1g, depending on their albedos and emissivities. Indeed, our calculations suggest that tidally driven outgassing rates of water vapor on these planets would be very similar to Europa's. Searches for rocky particles (i.e., SiO_2 dust), salts, and organics, all of which have been detected in Enceladus's plumes (see Hsu 2015), along with time-variable excesses of water vapor and its constituents in the spectra of these planets, could confirm the presence of explosive venting directly from potentially habitable subsurface oceans.

For the remainder of the cold ocean planets in this study, including Trappist-1h, oceans would lie >10 km beneath their surfaces so that liquid pockets perched in their ice shells would serve as the source of material ejected into space during cryovolcanic eruptions. If MOA-2007-BLG-192L b indeed has an internal ocean and cryovolcanism, this would be especially unique, as it would represent a potentially habitable cryovolcanically active planet orbiting a brown dwarf (Gould et al. 2010).

It must be noted that even in the case of planets such as MOA-2007-BLG-192L b, where oceans would be located beneath several tens of kilometers of surface ice, transient habitable environments could be maintained in their ice shells (see Ruiz et al. 2007). This may especially be the case for planets like GJ 514 b, HD33793 (Kapteyn c), and Trappist-1h, which have ice shells >10 km thick for a variety of assumptions but which also experience strong internal heating. Regardless of the depth to liquid water on these planets, potentially habitable liquid water reservoirs, including oceans, could exist on all of them. This is consistent with past work that suggested tidal heating could generate and maintain habitable subsurface oceans on ice-covered exoplanets (Vance et al. 2007; Jackson et al. 2008).

Of all the planets considered in this study, Proxima Cen b and LHS 1140 b are the most promising candidates for detectable cryovolcanism. Although the tidally driven outgassing rates of water vapor (in kg s^{-1}) are comparable to, or larger than, that of Europa for several other planets in our study, tidally driven cryovolcanism on these worlds could be difficult to detect, as the estimated amount of water vapor in their exospheres would exceed the amount of H_2O that would be released by tidally driven cryovolcanism by several orders of magnitude. Notwithstanding, if we also account for non–tidally driven cryovolcanism, such as cryovolcanism driven by radiogenic and other sources (e.g., induction heating, obliquity tides, etc.), given the relatively shallow depths to their possible ocean layers, cryovolcanism might be telescopically detected for all of the Kepler planets considered here.

These results suggest that, in order to understand the diversity of habitable worlds throughout our galaxy, searches for habitable environments should consider not only rocky exoplanets that lie in the stellar habitable zone but also the potential for habitable environments outside of the "Goldilocks Zone," even beyond the snow lines of exoplanetary systems. If the solar system is any guide, habitable exomoons with subsurface oceans could also be plentiful in our galaxy (Tjoa et al. 2020). Therefore, establishing the prospects for geological activity that would facilitate the cycling of water, energy, and organics in exoplanets themselves represents an important avenue for understanding the astrobiological significance of the expected diverse array of ocean worlds in our galaxy.

The upcoming Nancy Grace Roman Space Telescope is expected to discover over 1000 exoplanets on wide orbits (typically greater than ∼1 au) via microlensing (Penny et al. 2019), completing the exoplanet demographic census and providing constraints on the demographics of potential ocean planets. Roman could also potentially detect exomoons (Bachelet et al. 2022; Limbach et al. 2022). In the near term, analyses of observational data from the James Webb Space Telescope and design of the Habitable Worlds Observatory recommended by the Astro 2020 Decadal Survey (National Academies of Sciences, Engineering, & Medicine 2021) should be undertaken with these possibilities in mind.

Acknowledgments

L.C.Q. gratefully acknowledges funding support from NASA's Habitable Worlds Program (WBS: 811073.02.36.01.78). A.R. and G.T.M. acknowledge funding support from the University of Washington's Astrobiology Program and the Virtual Planetary Laboratory Team, a member of the NASA Nexus for Exoplanet System Science, funded via NASA Astrobiology Program grant No. 80NSSC18K0829. All authors acknowledge support from the NASA Goddard Science Task Group Program (WBS: 981698.01.04.51.05.60.72). We also thank Dr. Jason Barnes, whose comments and suggestions improved the quality of this manuscript.

ORCID iDs

Lynnae C. Quick https://orcid.org/0000-0003-0123-2797
Aki Roberge https://orcid.org/0000-0002-2989-3725
Guadalupe Tovar Mendoza https://orcid.org/0000-0001-5455-6678
Elisa V. Quintana https://orcid.org/0000-0003-1309-2904
Allison A. Youngblood https://orcid.org/0000-0002-1176-3391

References

Abramov, O., & Spencer, J. R. 2008, Icar, 195, 378
Abramov, O., & Spencer, J. R. 2009, Icar, 199, 189

Agol, E., Dorn, C., Grimm, S. L., et al. 2021, PSJ, 2, 1
Airapetian, V. S., Glocer, A., Khazanov, G. V., et al. 2017, ApJL, 836, L3
Anderson, J. D., Lau, E. L., Sjogren, W. L., Schubert, G., & Moore, W. B. 1997, Sci, 276, 1236
Anglada-Escudé, G., Amado, P. J., Barnes, J., et al. 2016, Natur, 536, 437
Anglada-Escudé, G., Arriagada, P., Tuomi, M., et al. 2014, MNRAS, 443, L89
Bachelet, E., Specht, D., Penny, M., et al. 2022, A&A, 664, A136
Baraffe, I., & Chabrier, G. 1996, ApJL, 461, L51
Baraffe, I., Chabrier, G., Barman, T. S., Allard, F., & Hauschildt, P. H. 2003, A&A, 402, 701
Baraffe, I., Chabrier, G., Allard, F., & Hauschildt, P. H. 1998, A&A, 337, 403
Baraffe, I., Chabrier, G., Allard, F., & Hauschildt, P. H. 2002, A&A, 382, 563
Barclay, T., Quintana, E. V., Adams, F. C., et al. 2015, ApJ, 809, 7
Barr, A. C., Dobos, V., & Kiss, L. L. 2018, A&A, 613, A37
Barr, A. C., & Pappalardo, R. T. 2005, JGRE, 110, E12005
Barr, A. C., & Showman, A. P. 2009, in Europa, ed. R. T. Pappalardo, W. B. McKinnon, & K. Khurana (Tucson, AZ: Univ. Arizona Press), 405
Barth, P., Carone, L., & Barnes, R. 2021, AsBio, 21, 1325
Bazot, M., Christensen-Dalsgaard, J., Gizon, L., & Benomar, O. 2016, MNRAS, 460, 1254
Beaulieu, J.-P., Bennett, D. P., Fouqué, P., et al. 2006, Natur, 439, 437
Beddingfield, C. B., & Cartwright, R. J. 2021, Icar, 367, 114583
Běhounková, M., Tobie, G., & Cadek, O. 2015, NatGe, 8, 601
Benneke, B. 2019, ApJL, 887, L14
Bennett, D. P., Bond, I. A., Udalski, A., et al. 2008, ApJ, 684, 663
Beyer, R. A., Spencer, J. R., McKinnon, W. B., et al. 2019, Icar, 323, 16
Bland, M. T., Singer, K. N., McKinnon, W. B., & Schenk, P. M. 2012, GeoRL, 39, L17204
Bolmont, E., Selsis, F., & Owen, J. E. 2017, MNRAS, 464, 3728
Borucki, W., Thompson, S. E., Agol, E., & Hedges, C. 2018, NewAR, 83, 28
Borucki, W. J., Agol, A., Fressin, F., Kaltenegger, L., et al. 2013, Sci, 340, 587
Bourrier, V., de Wit, J., Bolmont, E., et al. 2017, AJ, 154, 121
Budyko, M. I. 1969, Tell, 21, 611
Carnahan, E., Wolfenbarger, N. S., Jordan, J. S., & Hesse, M. E. 2021, E&PSL, 563, 116886
Carr, M. H., Belton, M. J. S., Chapman, C. R., Davies, M. E., et al. 1998, Natur, 391, 363
Cartwright, R. J., Beddingfield, C. B., Nordheim, T. A., et al. 2020, ApJL, 898, L22
Cassen, P. M., Reynolds, R. T., & Peale, S. J. 1979, GeoRL, 6, 731
Chen, E. M. A., Nimmo, F., & Glatzmaier, G. A. 2014, Icar, 229, 11
Chivers, C. J., Buffo, J. J., & Schmidt, B. E. 2021, JGRE, 126, e2020JE006692
Cloutier, R., Astudillo-Defru, N., Doyon, R., Bonfils, X., et al. 2017, A&A, 608, A35
Cochran, W. D., Fabrycky, D. C., Torres, G., Fressin, F., et al. 2011, ApJ, 197, 7
Craft, K., Patterson, G. W., Lowell, R. P., & Germanovich, L. 2016, Icar, 274, 297
Crawford, G. D., & Stevenson, D. J. 1988, Icar, 73, 66
Croft, S. K., & Soderblom, L. A. 1991, in Uranus, ed. J. T. Bergstralh et al. (Tucson, AZ: Univ. Arizona Press), 561
Cruikshank, D. P., Umurhan, O. M., Beyer, R. A., et al. 2019, Icar, 330, 155
Cruikshank, D. P., Dalle Ore, C. M., Scipioni, F., et al. 2021, Icar, 356, 113786
Damasso, M., Perger, M., Almenara, J. M., et al. 2022, A&A, 666, A187
Del Genio, A. D., Way, M. J., & Amundsen, D. S. 2019, AsBio, 19, 99
Ding, F., & Wordsworth, R. D. 2020, ApJL, 891, L18
Ehrenreich, D., & Cassan, A. 2007, AN, 328, 789
Ehrenreich, D., Lecavelier des Etangs, A., Beaulieu, J.-P., & Grasset, O. 2006, ApJ, 651, 535
Fabrycky, D. C., Lissauer, J. J., Ragozzine, D., et al. 2014, ApJ, 790, 146
Fagents, S. A. 2003, JGRE, 108, 5139
Fagents, S. A., Greeley, R., Sullivan, R. J., et al. 2000, Icar, 144, 54
Frank, E. A., Meyer, B. S., & Mojzsis, S. J. 2014, Icar, 243, 274
Fu, R., O'Connell, R. J., & Sasselov, D. D. 2010, ApJ, 708, 1326
Fulton, B. J., & Petigura, E. A. 2018, AJ, 156, 264
Gaeman, J., Hier-Majumder, S., & Roberts, J. H. 2012, Icar, 220, 339
Geissler, P. E. 2000, in Encyclopedia of Volcanoes, ed. H. Sigurdsson (New York: Academic), 785
Gillon, M., Triaud, A. H. M. J., Demory, B.-O., et al. 2017, Natur, 542, 456
Gizis, J. E. 1997, AJ, 113, 806
Glaze, L. S., Baloga, S. M., & Wilson, L. 1997, JGR, 102, 6099
Gould, A., Udalski, A., Shin, I.-G., et al. 2014, Sci, 345, 46
Gould, A., Dong, S., Bennett, D. P., et al. 2010, ApJ, 710, 1800
Green, A. P., Montési, L. G. J., & Cooper, C. M. 2021, JGRE, 126, e2020JE006677
Greenberg, R., Hoppa, G. V., & Tufts, B. R. 1999, Icar, 141, 263
Greene, T. P., Bell, T. J., Ducrot, E., et al. 2023, Natur, 618, 39
Grimm, S. L., Demory, B.-O., Gillon, M., et al. 2018, A&A, 613, A68
Guenther, E. W., & Kislyakova, K. G. 2020, MNRAS, 491, 3974
Hall, D. T., Feldman, P. D., McGrath, M. A., & Strobel, D. F. 1998, ApJ, 499, 475
Hall, D. T., Strobel, D. F., Feldman, P. D., McGrath, M. A., & Weaver, H. A. 1995, Natur, 373, 677
Hammond, N. P., Parmenteir, E. M., & Barr, A. C. 2018, JGRE, 123, 3105
Hand, K. P., Chyba, C. F., Priscu, J. C., Carlson, R. W., & Nealson, K. H. 2009, in Europa, ed. R. T. Pappalardo, W. B. McKinnon, & K. Khurana (Tucson, AZ: Univ. Arizona Press), 589
Hansen, C. J., Castillo-Rogez, J., Grundy, W., et al. 2021, PSJ, 2, 137
Hansen, C. J., Esposito, L., & Stewart, A. I. F. 2006, Sci, 311, 1422
Haywood, M. 2008, A&A, 482, 673
Heller, R., & Armstrong, J. 2014, AsBio, 14, 50
Hemingway, D. J., Iess, L., Tadjeddine, R., & Tobie, G. 2018, in Enceladus and the Icy Moons of Saturn, ed. P. M. Schenk et al. (Tucson, AZ: Univ. Arizona Press), 57
Hendrix, A. R., & Hansen, C. J. 2010, in IAU Symp. 263, Icy Bodies of the Solar System (Cambridge: Cambridge Univ. Press), 126
Henning, W. G., & Hurford, T. A. 2014, ApJ, 789, 30
Henning, W. G., Renaud, J. P., Saxena, P., et al. 2018, arXiv:1804.05110
Hobbs, P. V. 1974, Ice Physics (New York, NY: Oxford Univ. Press)
Hofgartner, J. D., Birch, S. P. D., Castillo, J., et al. 2022, Icar, 375, 114835
Howett, C. J. A., Spencer, R. J., Peral, J., & Segura, M. 2010, Icar, 206, 573
Hsu, H.-W., Postberg, F., Sekine, Y., et al. 2015, Natur, 519, 207
Hurford, T. A., Helfenstein, P., Hoppa, G. V., Greenberg, R., & Bills, B. G. 2007, Natur, 447, 292
Hurford, T. A., Henning, W. G., Maguire, R., et al. 2020, Icar, 338, 113466
Hussmann, H., Sohl, F., & Spohn, T. 2006, Icar, 185, 258
Hussmann, H., & Spohn, T. 2004, Icar, 171, 391
Hussmann, H., Spohn, T., & Wieczerkowski, K. 2002, Icar, 156, 143
Iess, L., Stevenson, D. J., Parisi, M., et al. 2014, Sci, 344, 78
Jackson, B., Barnes, R., & Greenberg, R. 2008, MNRAS, 391, 237
Jacobson, R. A., Campbell, J. K., Taylor, A. H., & Synnott, S. P. 1992, AJ, 103, 2068
Jankowski, D. G., & Squyres, S. W. 1988, Sci, 241, 1322
Jin, S., Mordasnini, C., & Parmentier, V. 2014, ApJ, 795, 65
Journaux, B., Daniel, I., & Petitgirard, S. 2017, E&PSL, 463, 36
Journaux, B., Kalousová, K., Sotin, C., et al. 2020, SSRv, 216, 7
Kaltenegger, L., Sasselov, D., & Rugheimer, S. 2013, ApJL, 775, L47
Kane, S. R., Arney, G. N., Byrne, P. K., et al. 2021, JGRE, 126, e2020JE006643
Khodachenko, M. L., Ribas, I., Lammer, H., et al. 2007, AsBio, 7, 167
Kislyakova, K. G., Fossati, L., Johnstone, C. P., et al. 2018, ApJ, 858, 105
Kislyakova, K. G., Noack, L., Johnstone, C. P., et al. 2017, NatAs, 1, 878
Kivelson, M. G., Khurana, K. K., & Russell, C. T. 2000, Sci, 289, 1340
Kozai, Y. 1968, BGeod, 89, 355
Krissansen-Totton, J., & Fortney, J. J. 2022, ApJ, 933, 115
Krissansen-Totton, J., Galloway, M. L., Wogan, N., Dhaliwal, J. K., & Fortney, J. J. 2021, ApJ, 913, 107
Kubas, D., Beaulieu, J. P., Bennett, D. P., et al. 2012, A&A, 540, A78
Kubas, D., Cassan , A., Dominik, M., et al. 2008, A&A, 483, 317
Lammer, H., Odert, P., Leitzinger, M., et al. 2009, A&A, 506, 399
Le Gall, A., Leyrat, C., Janssen, M., et al. 2017, NatAs, 1, 0063
Léger, A., Selsis, F., Sotin, C., et al. 2004, Icar, 169, 499
Lellouch, E., Ali-Dib, M., & Jessup, K.-L. 2015, Icar, 253, 99
Lesage, E., Massol, H., & Schmidt, F. 2020, Icar, 335, 113369
Levi, A., Sasselove, D., & Podolak, M. 2013, ApJ, 769, 29
Levi, A., Sasselove, D., & Podolak, M. 2014, ApJ, 792, 125
Lillo-Box, J., Figueira, P., Leleu, A., et al. 2020, A&A, 642, A121
Limbach, M. A., Vos, J. M., Soares-Furtado, M., et al. 2022, BAAS, 54, 183
Lopes, R. M. C., Kirk, R. L., Mitchell, K. L., et al. 2013, JGRE, 118, 416
Lopes, R. M. C., Kamp, L. W., Smythe, W. D., et al. 2004, Icar, 169, 140
Lopez, E. D. 2017, MNRAS, 472, 245
Luger, R., & Barnes, R. 2015, AsBio, 15, 119
Luger, R., Sestovic, M., Kruse, E., et al. 2017, NatAs, 1, 0129
Mamajek, E. E. 2022, A Modern Mean Dwarf Stellar Color and Effective Temperature Sequence. Version 2022.04.16, http://www.pas.rochester.edu/~emamajek/EEM_dwarf_UBVIJHK_colors_Teff.txt
Manga, M., & Michaut, C. 2017, Icar, 286, 261
Manga, M., & Wang, C.-Y. 2007, GeoRL, 34, L07202
Martin, C. R., & Binzel, R. P. 2021, Icar, 356, 113763
Mascareño, A. S., Faria, J. P., Figueira, P., et al. 2020, A&A, 639, A77
Matson, D. L., Castillo-Rogez, J. C., Davies, A. G., & Johnson, T. V. 2012, Icar, 221, 53

McEwen, A. S., Keszthelyi, L. P., Lopes, R., Schenk, P. M., & Spencer, J. R. 2004, in Jupiter: The Planet, Satellites, and Magnetosphere, ed. F. Bagenal, T. Dowling, & W. McKinnon (Cambridge: Cambridge Univ. Press), 307
McGovern, P. J., White, O. L., & Schenk, P. M. 2021, JGRE, 126, e2021JE006964
McGrath, M. A., Lellouch, E., Strobel, D. F., Feldman, P. D., & Johnson, R. E. 2004, in Jupiter: The Planet, Satellites, and Magnetosphere, ed. F. Bagenal, T. Dowling, & W. McKinnon (Cambridge: Cambridge Univ. Press), 457
McKinnon, W. B. 1999, GeoRL, 26, 951
Ment, K., Dittmann, J. A., Astudillo-Defru, N., et al. 2019, AJ, 157, 32
Millholland, S., & Laughlin, G. 2019, NatAs, 3, 424
Moore, J. M., McKinnon, W. B., Spencer, J. R., et al. 2016, Sci, 351, 1284
Moore, W. B. 2003, JGRE, 108, 5096
Muñoz-Iglesias, V., Bonales, L. J., & Prieto-Ballesteros, O. 2013, AsBio, 13, 693
National Academies of Sciences, Engineering, and Medicine 2021, Pathways to Discovery in Astronomy and Astrophysics for the 2020s. (Washington, DC: The National Academies Press)
Nimmo, F. 2020, PNAS, 117, 16107
Nimmo, F., Barr, A. C., Behounková, M., & McKinnon, W. B. 2018, in Enceladus and the Icy Moons of Saturn, ed. P. M. Schenk et al. (Tucson, AZ: Univ. Arizona Press), 79
Nimmo, F., & Pappalardo, R. T. 2016, JGRE, 121, 1378
Nimmo, F., Pappalardo, R. T., & Giese, B. 2003, Icar, 166, 21
Noack, L., Kislyakova, K. G., Johnstone, C. P., Güdel, M., & Fossati, L. 2021, A&A, 651, A103
O'Brien, D. P., Geissler, P., & Greenberg, R. 2002, Icar, 156, 152
Ojakangas, G. W., & Stevenson, D. J. 1989, Icar, 81, 220
Owen, J. E., & Wu, Y. 2013, ApJ, 775, 105
Oza, A. V., Johnson, R. E., Lellouch, E., et al. 2019, ApJ, 885, 168
Paganini, L., Villanueva, G. L., & Roth, L. 2020, NatAs, 4, 266
Paradise, A., Menou, K., Valencia, D., & Lee, C. 2019, JGRE, 124, 1
Peale, S. J., Cassen, P., & Reynolds, R. T. 1979, Sci, 203, 892
Pecaut, M. J., & Mamajek, E. E. 2013, ApJS, 208, 9
Penny, M. T., Gaudi, B. S., & Kerins, E. 2019, ApJS, 241, 3
Phillips, C. B., McEwen, A. S., Hoppa, G. V., et al. 2000, JGR, 105, 22579
Pierrehumbert, R., & Gaidos, E. 2011, ApJL, 734, L13
Porco, C. C., Helfenstein, P., Thomas, P. C., et al. 2006, Sci, 311, 1393
Postberg, F., Kempf, S., Schmidt, J., et al. 2009, Natur, 459, 1098
Postberg, F., Khawaja, N., Abel, B., et al. 2018, Natur, 558, 564
Postberg, F., Schmidt, J., Hillier, J., Kempf, M., & Srama, R. 2011, Natur, 474, 620
Quick, L. C., Adams, E., & Barr, A. C. 2017, in Planetary Science Vision 2050 Workshop 1989 (Houston, TX: The Lunar and Planetary Institute), 8036
Quick, L. C., Barnouin, O. S., Prockter, L. M., & Patterson, G. W. 2013, P&SS, 86, 1
Quick, L. C., Buczkowski, D. B., Ruesch, O., et al. 2019, Icar, 320, 119
Quick, L. C., Fagents, S. A., Nuñez, K. A., et al. 2021, in 52nd Lunar and Planetary Science Conf., 2548 (Houston, TX: The Lunar and Planetary Institute), 2637
Quick, L. C., Fagents, S. A., & Núñez, K. A. 2022, Icar, 387, 115185
Quick, L. C., & Hedman, M. M. 2020, Icar, 343, 113667
Quick, L. C., & Marsh, B. D. 2015, Icar, 253, 16
Quick, L. C., & Marsh, B. D. 2016, JVGR, 319, 66
Quick, L. C., Roberge, A., Barr Mlinar, A., & Hedman, M. M. 2020, PASP, 132, 084401
Ramirez, R. M., & Kaltenegger, L. 2014, ApJL, 797, L25
Rathbun, J. A., Spencer, J. R., & Tamppari, L. K. 2004, Icar, 169, 127
Rhoden, A. R., Hurford, T. A., Roth, L., & Retherford, K. 2015, Icar, 253, 169
Ribas, I., Tuomi, M., Reiners, A., et al. 2018, Natur, 563, 365
Ribas, I., Bolmont, E., Selsis, F. , et al. 2016, A&A, 596, A11
Roberts, J. H., & Nimmo, F. 2008, Icar, 194, 675
Rogers, L. A. 2015, ApJ, 801, 41
Roth, L. 2021, GeoRL, 48, e2021GL094289
Roth, L., Retherford, K. D., & Saur, J. 2014b, PNAS, 111, E5123
Roth, L., Saur, J., & Retherford, K. D. 2014a, Sci, 343, 171
Ruesch, O., Genova, A., Neumann, W., et al. 2019, NatGe, 12, 505
Ruesch, O., Platz, T., Schenk, P., et al. 2016, Sci, 353, 6303
Ruiz, J. 2003, Icar, 166, 436
Ruiz, J., Montoya, L., López, V., & Amils, R. 2007, OLEB, 37, 287
Safonova, M., Murthy, J., & Shchekinov, Y. A. 2016, IJAsB, 15, 93
Sagan, C., & Mullen, G. 1972, Sci, 177, 52
Schenk, P. M. 1991, JGR, 96, 1887
Schmidt, B. E., Blankenship, D. D., Patterson, G. W., & Schenk, P. M. 2011, Natur, 479, 502
Schubert, G., Anderson, J. D., Spohn, T., & McKinnon, W. B. 2004, in Jupiter: The Planet, Satellites, and Magnetosphere, ed. F. Bagenal, T. Dowling, & W. McKinnon (Cambridge: Cambridge Univ. Press), 281
Seager, S., Kuchner, M., Hier-Majumder, C. A., & Militzer, B. 2007, ApJ, 669, 1279
Sellers, W. D. 1969, JApMe, 8, 392
Shematovich, V. I., Johnson, R. E., Cooper, J. F., & Wong, M. C. 2005, Icar, 173, 480
Singer, K. N., White, O. L., Schmitt, B., et al. 2022, NatCo, 13, 1542
Smith, B. A., Soderblom, L. A., Banfield, D., et al. 1989, Sci, 246, 1422
Snellen, I. A. G., Désert, J.-M., Waters, L. B. F. M., et al. 2017, AJ, 154, 77
Soderblom, L. A., Kieffer, S. W., & Becker, T. L. 1990, Sci, 19, 410
Sotin, C., Head, J. W., III, & Tobie, G. 2002, GeoRL, 29, 1233
Sparks, W. B., Hand, K. P., & McGrath, M. A. 2016, ApJ, 829, 121
Sparks, W. B., Schmidt, B. E., & McGrath, M. A. 2017, ApJL, 839, L18
Spencer, J. R., Barr, A. C., Esposito, L. W., et al. 2009, in Saturn from Cassini-Huygens, ed. M. K. Dougherty, L. W. Esposito, & S. M. Krimigis (Berlim: Springer), 683
Spencer, J. R., Pearl, J. C., Segura, M., et al. 2006, Sci, 311, 1401
Spencer, J. R., Tamppari, L. K., Martin, T. Z., & Travis, L. D. 1999, Sci, 284, 1514
Stacey, F. D., & Davis, P. M. 2008, Physics of the Earth (Cambridge: Cambridge Univ. Press)
Stassun, K. G., Oelkers, R. J., Paegert, M., et al. 2019, AJ, 158, 138
Stern, S. A. 1999, RvGeo, 37, 453
Stevenson, D. J. 1982, P&SS, 30, 755
Tajika, E. 2008, ApJL, 680, L53
Tamburo, P., Mandell, A., Deming, D., & Garhart, E. 2018, AJ, 155, 221
Teolis, B. D., Wyrick, D. Y., Bouquet, A., Magee, B. A., & Waite, J. H. 2017, Icar, 284, 18
Thomas, P. C., Tajeddine, R., Tiscareno, M. S., et al. 2016, Icar, 264, 37
Tjoa, J. N. K. Y., Mueller, M., & van der Tak, F. F. S. 2020, A&A, 636, A50
Tobie, G., Choblet, G., & Sotin, C. 2003, JGR, 108, 5124
Torres, G., Kipping, D. M., Fressin, F., et al. 2015, ApJ, 800, 99
Torres, G., Kane, S. R., Rowe, J. F., et al. 2017, AJ, 154, 264
Tsiaras, A., Waldmann, I. P., Tinetti, G., Tennyson, J., & Yurchenko, S. N. 2019, NatAs, 3, 1086
Turbet, M., Leconte, J., Selsis, F., & Anglada-Escudé, S. N. 2016, A&A, 596, A112
Vance, S., Barnes, R., Brown, J. M., et al. 2015, in 46th Lunar and Planetary Science Conf. 1832 (Houston, TX: The Lunar and Planetary Institute), 2717
Vance, S., Harnmeijer, J., & Kimura, J. 2007, AsBio, 7, 987
Vance, S. D., Barnes, R. K., & Journaux, B. 2020, in Exoplanets in Our Backyard 2195 (Houston, TX: The Lunar and Planetary Institute), 3069
Verbiscer, A., French, R., Showalter, M., & Helfenstein, P. 2007, Sci, 315, 815
Watson, A. J., Donahue, T. M., & Walker, J. C. G. 1981, Icar, 48, 150
Wilhelm, C., Barnes, R., Deitrick, R., & Mellman, R. 2022, PSJ, 3, 13
Wolf, E. T. 2017, ApJL, 839, L1
Yang, J., Ding, F., & Ramirez, R. M. 2017, NatGe, 10, 556
Yelle, R. V. 2004, Icar, 170, 167